Yersinia actively downregulates type III secretion and adhesion at higher cell densities

Francesca Ermoli[1], Gabriele Malengo[2,3], Christoph Spahn[4,5], Timo Glatter[6] & Andreas Diepold[1,3,7]

1: Department of Ecophysiology, Max Planck Institute for Terrestrial Microbiology, Marburg, Germany

2: Core Facility for Flow Cytometry and Imaging, Max Planck Institute for Terrestrial Microbiology, Marburg, Germany

3: Center for Synthetic Microbiology (SYNMIKRO), Marburg, Germany

4: Department of Natural Products in Organismic Interactions, Max Planck Institute for Terrestrial Microbiology, Marburg, Germany

5: Rudolf Virchow Center for Translational Bioimaging, Julius-Maximilians-University Würzburg, Würzburg, Germany

6: Core Facility for Mass Spectrometry and Proteomics, Max Planck Institute for Terrestrial Microbiology, Marburg, Germany

7: Department of Applied Biology, Institute of Applied Biosciences, Karlsruhe Institute of Technology (KIT), Karlsruhe, Germany

Corresponding author:

Andreas Diepold, andreas.diepold@kit.edu, +49-721-60845610

Short title: *Yersinia* downregulates type III secretion and adhesion at higher densities

Abstract

The T3SS injectisome is used by Gram-negative bacteria, including important pathogens, to manipulate eukaryotic target cells by injecting effector proteins. While in some bacterial species, T3SS-negative bacteria benefit from the activity of their T3SS-positive siblings, the T3SS model organism *Yersinia enterocolitica* was thought to uniformly express and assemble injectisomes. In this study, we found that *Yersinia* actively suppress T3SS expression, assembly and activity at higher cell densities, such as inside microcolonies. This effect is highly specific to the T3SS, reversible, and distinct from stationary phase adaptation. It is conferred by the main T3SS transcription factor VirF, which is downregulated at higher densities and whose *in trans* expression restores T3SS activity. Transcript analysis showed that this effect is mediated by increased levels of the regulatory RNAs CsrBC, which sequester the regulatory protein CsrA and destabilize the *virF* transcript. The concomitant downregulation of the VirF-dependent adhesin YadA led to a drastic reduction in bacterial cell adhesion. We propose that this active suppression of T3SS secretion and cell attachment at higher local bacterial densities promotes a switch during *Yersinia* infection from a T3SS-active colonization stage to a bacterial replication and dissemination phase.

18 **Introduction**

19 To manipulate eukaryotic cells, many Gram-negative bacteria, including important human pathogens, use
20 a type III secretion system, which allows to inject effector proteins into target cells in a one-step
21 mechanism [1–4]. These effector proteins can exert a wide variety of functions that facilitate survival and
22 proliferation of the respective bacteria according to their infection route and lifestyle [5–7]. In contrast,
23 the T3SS machinery, also known as injectisome, is highly conserved. It consists of a set of ring structures
24 that anchor the injectisome in the bacterial membranes and surround an export apparatus in the inner
25 membrane (IM), thought to act as a gating structure [8,9]. A hollow needle structure forms a conduit for
26 the effectors, which is connected to a translocon pore in the target cell membrane (Fig. 1a). At the cytosolic
27 interface of the injectisome, a set of conserved cytosolic components form six pod structures [10–14] that
28 shuttle effectors between the injectisome and the cytosol in *Yersinia enterocolitica* [15–17].

29 Expression, assembly and activity of the T3SS are tightly regulated. Often, expression and assembly only
30 occur within the host organism. In *Yersinia*, this is based on an RNA thermometer structure in the
31 transcript of the main transcriptional activator of the T3SS, called VirF in *Y. enterocolitica* and LcrF in
32 *Y. pseudotuberculosis* and *Y. pestis* [18,19]. While expression of VirF is sufficient for the formation of
33 injectisomes, a second signal, host cell contact, is required to activate secretion. This activation, which can
34 be mimicked by Ca^{2+} depletion or absence of the gatekeeper protein SctW in *Yersinia* [20,21], also removes
35 the secreted posttranscriptional repressors YscM1/2 (LcrQ in *Y. pseudotuberculosis*) [22,23], leading to an
36 upregulated production of the structural components and especially effectors of the system [23–25].
37 Recent studies in *Y. pseudotuberculosis* revealed additional layers of regulation (reviewed in [26]), such as
38 the CsrABC system, where CsrA, which positively regulates T3SS expression by stabilizing the *virF*
39 transcript, is sequestered by the two regulatory RNAs CsrB and CsrC [27].

40 This tight regulation of T3SS expression and activity may be required because of a phenomenon called
41 secretion-associated growth inhibition (SAGI), in which secreting bacteria greatly reduce their growth and
42 division. It was this striking phenotype that initially led to the discovery of the T3SS, when researchers
43 noted a specific growth inhibition of virulent *Yersinia* (now known to be equivalent to the presence of the
44 T3SS) at 37°C (T3SS expression) in the absence of Ca^{2+} (T3SS activation) [28–33]. Besides *Yersinia*, SAGI has
45 been shown to occur in two other main T3SS model organisms, *Salmonella enterica* and *Shigella flexneri*
46 [34–36]. However, it is still unclear if SAGI is a mere consequence of the energy expenditure for synthesis
47 and export of the T3SS machinery and effectors, or whether it is an actively regulated phenotype, as
48 suggested by the fact that growth and division are reinitiated very quickly, once secretion is stopped [37].

49 Given that the propagation of actively secreting bacteria is impeded, a differential expression of the T3SS
50 within the population is conceivably beneficial in some situations. Indeed, it was shown that the SPI-1
51 T3SS, used by *Salmonella enterica* to induce a strong inflammation in the host gut that clears competing
52 bacteria, is only active in a subset of bacteria, allowing the T3SS-inactive subpopulation to rapidly populate

53 the infection niche [34,38]. Similarly, *Pseudomonas aeruginosa* expresses its T3SS in a bistable way [39–
54 42]. In contrast, *Shigella flexneri* and *Yersinia enterocolitica*, where presence of the T3SS mainly gives a
55 benefit to individual cells (invasion of the cytosol of epithelial cells and evasion of the immune response,
56 respectively) [37,43], were so far found to be completely T3SS-positive, both in terms of expression and
57 assembly of injectisomes [42,44–46] and their activation [47].

58 However, these results were gained under standard laboratory conditions typically focusing on the
59 establishment of an infection at low bacterial densities. It is conceivable that this picture changes under
60 conditions mimicking later stages of infection, where bacteria may benefit from suppressing T3SS assembly
61 and activity, allowing them to replicate extracellularly in their established niches or to disseminate.
62 Increased local bacterial density, a common aspect of later-stage infection environments, might therefore
63 influence the activity of the T3SS.

64 In this study, we tested this hypothesis and found that T3SS assembly, activation, and bacterial adhesion
65 are governed by cell density. This effect is clearly displayed in *Y. enterocolitica* microcolonies, where only
66 a thin layer of cells at the rim of the colony are T3SS-positive, but can also be replicated and analyzed in
67 liquid cultures. The density-driven downregulation of the T3SS is reversible, highly specific, and distinct
68 from stationary phase adaptation. A >10 times increased concentration of the regulatory RNA CsrC at
69 higher bacterial densities leads to sequestration of the RNA-binding protein CsrA and downregulation of
70 expression of the main T3SS transcription factor VirF. Accordingly, expression of VirF *in trans* overrides the
71 effect. We propose that the highly specific T3SS regulatory phenotype discovered in this study increases
72 the chances of bacterial dissemination during and after infection by creating a T3SS-negative, non-
73 adhesive subpopulation that can replicate and disseminate.

74

Results

Type III secretion activity is confined to the edges of *Y. enterocolitica* microcolonies

To investigate the regulation of T3SS activity under conditions relevant at later stages of infection, we imaged microcolonies of *Y. enterocolitica* Δ*sctW* at host temperature (37°C). T3SS activation can be monitored using the strong upregulation of the effector YopE upon T3SS activation [47–50]. To ensure a high sensitivity and temporal resolution of the reporter, we used the fast-folding fluorescent protein sfGFP with a SsrA degradation tag [51]. The resulting P_{yopE}-*sfGFP-ssrA* reporter system allowed for accurate temporal mapping of T3SS activation (Suppl. Fig. 1). Strikingly, confocal microscopy scanning of the microcolony showed T3SS activation exclusively at the periphery of the colony (Fig. 1b, Suppl. Fig. 2), suggesting a strong repression of secretion towards the center.

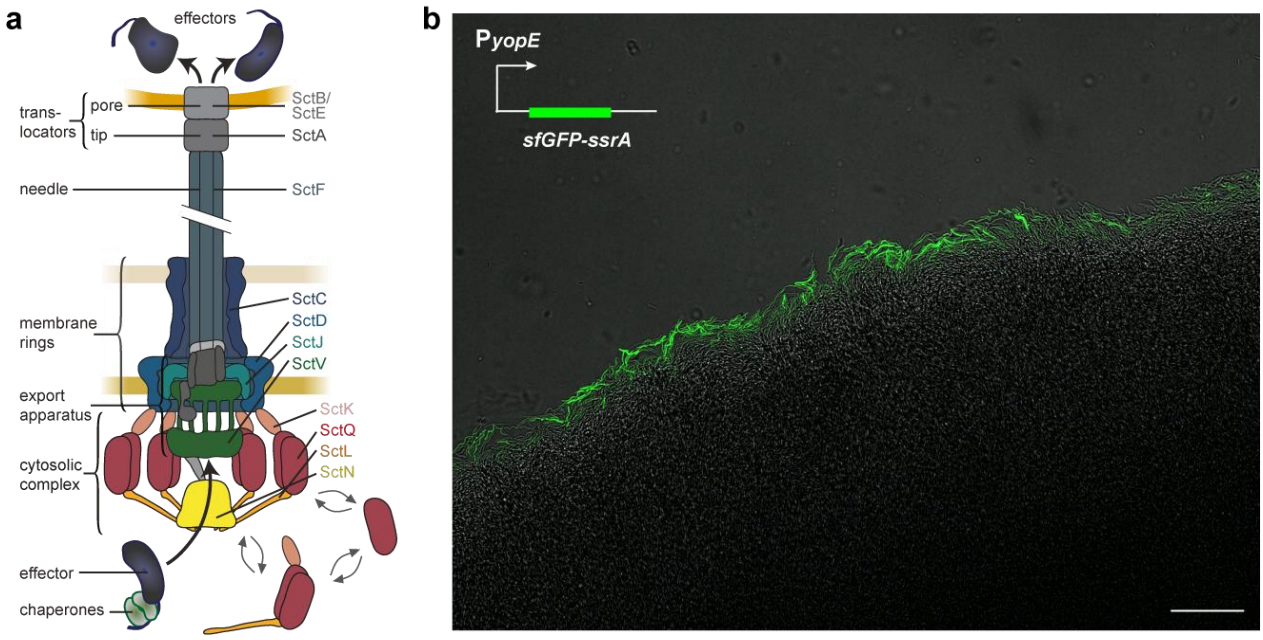

Fig. 1 –T3SS activation is only detected at the edge of *Y. enterocolitica* microcolonies.

a) Schematic depiction of the T3SS injectisome (adapted from [52]); right, common nomenclature names of main T3SS components [53,54]. **b)** Confocal microscopy image of a *Y. enterocolitica* Δ*sctW* P_{yopE}-*sfGFP-ssrA* microcolony section at 37°C. T3SS activity, which results in a strong upregulation of the *yopE* promoter and cellular fluorescence, is only detected at the edge of the microcolony. Scale bar, 50 µm, *n*=3.

92 **Type III assembly and activity are affected by bacterial cell density**

93 To investigate if the spatial regulation of T3SS activation observed in Fig. 1b was linked to the different cell
94 densities perceived across the microcolony, we tested the effector secretion of *Y. enterocolitica* liquid
95 cultures incubated under secreting conditions (37°C, low [Ca^{2+}]) at increasing cell densities. As *Y.*
96 *enterocolitica* can reach optical densities at 600 nm (OD_{600}) of 15-20, the ODs at the inoculum (OD_{in}) used
97 in this experiment correspond to the exponential phase growth in non-secreting bacteria (Suppl. Fig. 3).
98 Cultures inoculated to an initial OD_{600} of 0.1 (OD_{in}=0.1), a condition regularly used for secretion
99 experiments [42,47,48,55], which we refer to as reference hereafter, secreted large amounts of effector
100 proteins. Increasing densities gradually reduced secretion levels, up to a complete inhibition of T3SS
101 function at higher bacterial densities (OD_{in}=1.5) (Fig. 2a). This establishes an inverse correlation between
102 T3SS secretion and cell density. To describe this unexpected phenotype in more detail, we next tested
103 T3SS activation over time by quantifying the P_{yopE}-*sfGFP-ssrA* activity. In line with the previous results, the
104 reporter showed a weaker and shorter T3SS activation with increasing bacterial densities, again up to a
105 complete loss of activation at higher densities (Fig. 2b, Suppl. Fig. 4). To determine whether already the
106 assembly of the T3SS machinery was impacted by cell density, the number of injectisomes was quantified
107 by fluorescence microscopy at a single-cell level in a strain expressing a functional EGFP-SctQ fusion [44].
108 The analysis showed a significant reduction in the number of fluorescent foci corresponding to assembled
109 injectisomes at higher densities when compared to the reference (Fig. 2c). Like protein secretion itself,
110 T3SS assembly was almost fully repressed at higher cell densities. As expected, a certain degree of
111 heterogeneity was observed under all conditions tested, but neither a bimodal distribution, nor distinct
112 subpopulations were observed for T3SS assembly or activation in single-cell experiments (Fig. 2cd),
113 indicating a general downregulation of the T3SS. The results highlight a strong inverse relationship
114 between cell density and T3SS assembly and activation, which we refer to as density-dependent
115 downregulation of the T3SS (d^3T3).

116

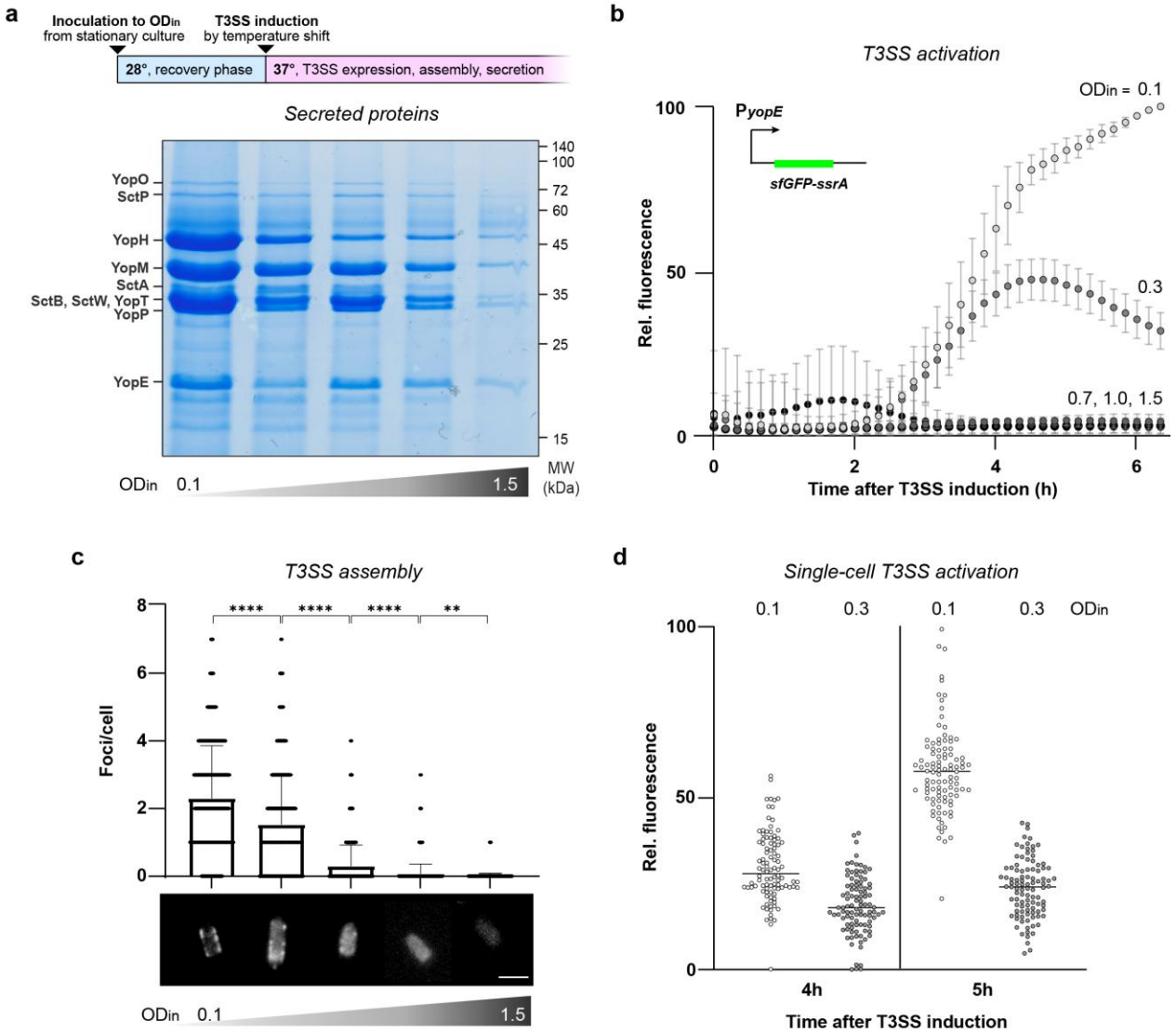

Fig. 2 – Assembly and activity of the T3SS are significantly reduced at higher bacterial densities.

a) Top, graphical depiction of secretion assay; bottom, effectors secreted by the T3SS at increasing OD_{in} (left to right: 0.1, 0.3, 0.7, 1.0, 1.5). Left, assignment of effectors; right, molecular weight (MW) standards. **b)** T3SS reporter assay (P_{yopE}-*sfGFP-SsrA*) [47,56] at increasing OD_{in} values as in a). Intensities are adjusted for OD_{600} and displayed relative to the highest OD-adjusted intensity value, growth curves of cultures used in these experiments are displayed in Suppl. Fig. 5. **c)** Quantification of EGFP-SctQ foci per bacterium, corresponding to assembled injectisomes, visualized by fluorescence microscopy at increasing OD_{in} as in b). Number of measurements and foci counts listed in Suppl. Table 1. Sample micrographs depicted at bottom, scale bar, 2 µm. **d)** Single-cell T3SS reporter assay (P_{yopE}-*sfGFP-SsrA*) of *Yersinia* cells to assay the heterogeneity of T3SS activation at the indicated low and intermediate activation levels (OD_{in}=0.1, 0.3, as indicated). Measurements were taken 4h and 5h post-secretion induction, intensities are displayed as in b). Each dot represents a single cell, black bars represent the average fluorescence intensity. *n*=3 for all panels. Gel image in a) shows representative result; for c, *n cells* = 300; for d, *n cells* = 100, statistical analysis was performed using a non-parametric t-test, ****, $p<0.0001$, whiskers denote standard deviation.

133 **The density-dependent T3SS inhibition is specific and reversible**

134 To probe if the observed correlation between bacterial density and the T3SS is specific or part of a more
135 global regulatory effect, we compared the total proteome of bacteria with OD_{in}=1.5 to the reference
136 (OD_{in}=0.1). Remarkably, 24 of the 25 most strongly downregulated proteins were directly T3SS-related
137 (marked by red dots in Fig. 3a), showing that the effect is highly specific for the T3SS. All T3SS proteins
138 were highly downregulated (3-256-fold, p<0.001 for all detected components), except for the negative
139 regulators YscM1 and YscM2, which were upregulated, and their chaperone SycH, whose expression
140 remained stable (Fig. 3a, Table 1). All T3SS gene classes – structural components, regulators, effectors and
141 chaperones – were similarly affected (Suppl. Fig. 6, Table 1). In contrast, expression of other proteins
142 encoded on the pYV virulence plasmid was largely unaltered (Suppl. Table 2). This indicates that the
143 downregulation is not caused by a change in plasmid copy number or overall protein expression from the
144 plasmid. Instead, it suggests a direct effect of bacterial densities on T3SS expression that is distinct from
145 stationary phase responses occurring at higher density. In line with this interpretation, proteins involved
146 in stationary phase response, which are highly expressed at stationary phase, were not significantly
147 upregulated at OD_{in}=1.5 (Suppl. Table 3). Taken together, our data unanimously point towards a specific
148 T3SS repression mechanism driven by cell density rather than a broader cellular reorganization.

149 We then tested if the d^3T3 effect is reversible. Bacterial cultures were inoculated at reference or higher
150 OD (OD_{in}=0.1 or 1.5) and then concentrated or diluted to the OD of the respective other culture prior to
151 induction of T3SS expression by a temperature shift to 37°C in the absence of Ca^{2+}. Bacteria were
152 resuspended in their respective centrifugation supernatant to avoid possible effects of fresh medium on
153 the analysis. Activation of the T3SS was measured as P_{yopE}-*sfGFP-ssrA* reporter activity for single bacteria.
154 Increasing the density of initially dilute cultures strongly suppressed T3SS activation. Likewise, diluting the
155 initially more concentrated cultures almost completely restored T3SS activation (Fig. 3b). We also tested
156 a possible role of the medium composition (e.g. by limitation of nutrients or presence of extracellular
157 negative regulators at higher densities) and found that secretion was neither strongly reduced at low
158 density by spent medium from high-density cultures, nor activated at high densities by fresh medium (Fig.
159 3c). Together, these results highlight a direct and reversible influence of bacterial density on T3SS
160 secretion.

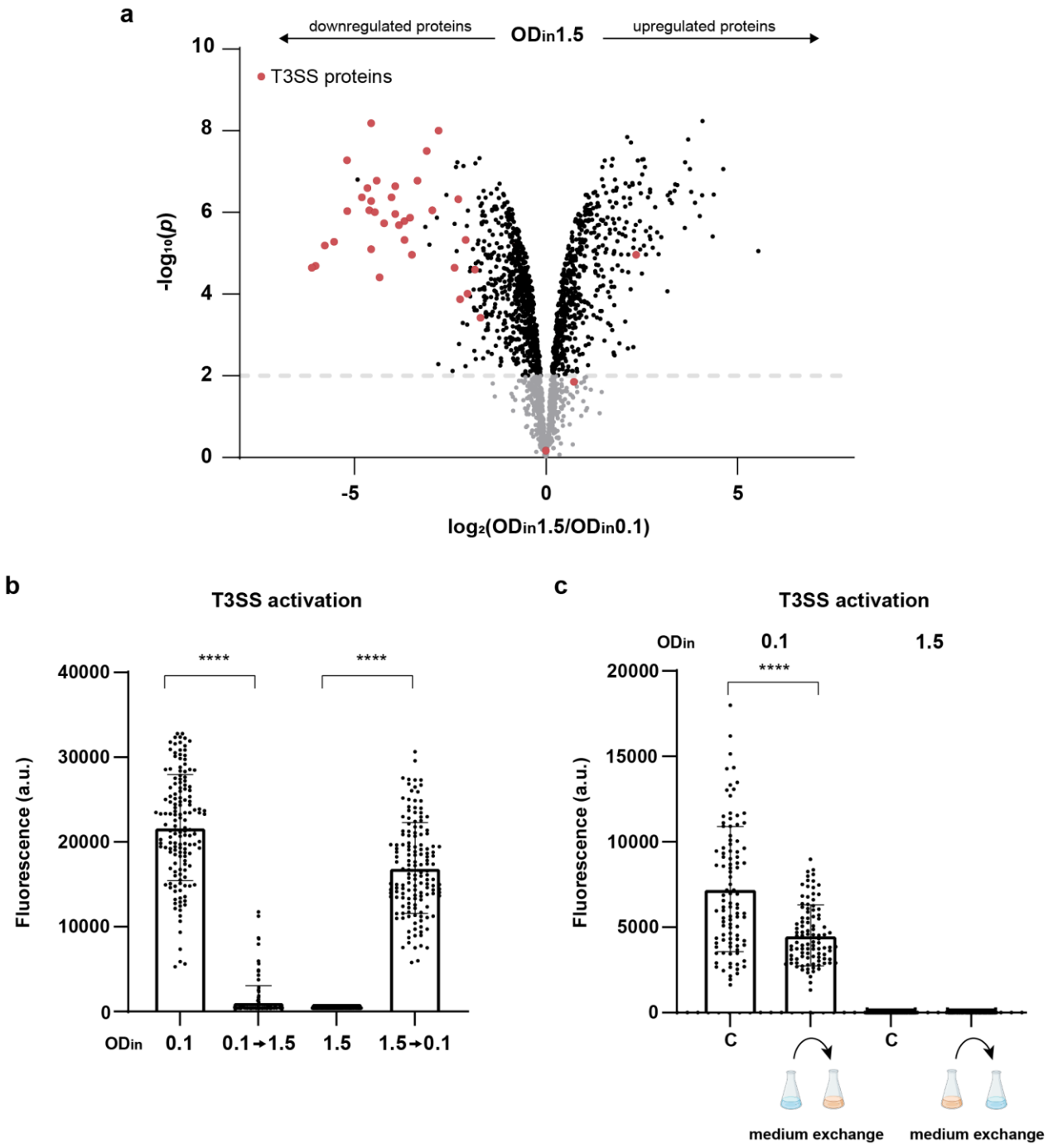

Fig. 3 – The density-dependent downregulation of the T3SS is specific and reversible.

a) Volcano plot showing differences in the expression of *Y. enterocolitica* proteins between cultures grown under secreting conditions at OD_{in} 1.5 and 0.1. All proteins with at least three detected peptides under both conditions are displayed; T3SS-related proteins are marked by larger red dots. **b)** T3SS reporter assay (P_{yopE}-*sfGFP-ssrA*) in strains with OD_{in}=0.1 or 1.5 and concentration or dilution at the time of the temperature shift to 37°C, as indicated. Measurements were performed 150 min after dilution/concentration. **c)** T3SS reporter assay (P_{yopE}-*sfGFP-ssrA*) in strains with OD_{in} values as indicated. Medium exchange at the time of the temperature shift to 37°C as depicted; C indicates constant incubation without medium change. Measurements were performed 150 min after medium exchange. *n*=3 biological replicates for all panels. In panels b) and c), *n cells* = 150, each spot represents a single measurement, whiskers denote standard deviation. Statistical analysis was performed using a non-parametric t-test; ****, $p<0.0001$.

174 **Global stationary phase regulators have a minor effect on T3SS assembly and function**

175 We next aimed to determine the cause for the previously unknown regulatory phenotype described above.
176 To investigate a possible role of known density-dependent global regulators of bacterial physiology and
177 behavior in the d^3T3, we studied the influence of quorum sensing (QS), the stationary phase/stress
178 response alternative sigma factor RpoS, and the stringent response regulators RelA and SpoT. In *Yersinia*,
179 both homologs of LuxI/R (*yenI/R*) and LuxS have been characterized, although no clear evidence of
180 functional LuxS-dependent AI-2 signaling has been provided so far. While QS in *Yersinia* influences, among
181 others, motility and biofilm formation [56–58], its role in bacterial virulence is less clear. We performed a
182 secretion assay in a *Y. enterocolitica* QS double mutant lacking the genes for YenI and the AI-2 kinase LsrK.
183 The secretion pattern of the mutant showed no significant impact of QS on secretion under the conditions
184 tested (Fig. 4a, Suppl. Fig. 7). Next, we tested the influence of the stationary phase/stress response RNA
185 polymerase sigma factor RpoS on d^3T3. RpoS is known to positively regulate motility and biofilm formation
186 in many Gram-negative bacteria [59,60], but its impact on *Yersinia* virulence is unclear. The activity of the
187 T3SS at OD_{in} 0.1 and 1.5 was not influenced by the deletion or overexpression of RpoS (Fig. 4b). Finally, we
188 tested the role of RelA [61,62] and SpoT [63,64], activators of the stringent response, which is a key process
189 in stationary phase adaptation. Similar to the previous experiments, deletion of RelA or SpoT did not
190 restore secretion at higher bacterial densities (Suppl. Fig. 8). These results further support the hypothesis
191 that the d^3T3 is a specific phenotype rather than a part or consequence of stationary phase adaptation.

192 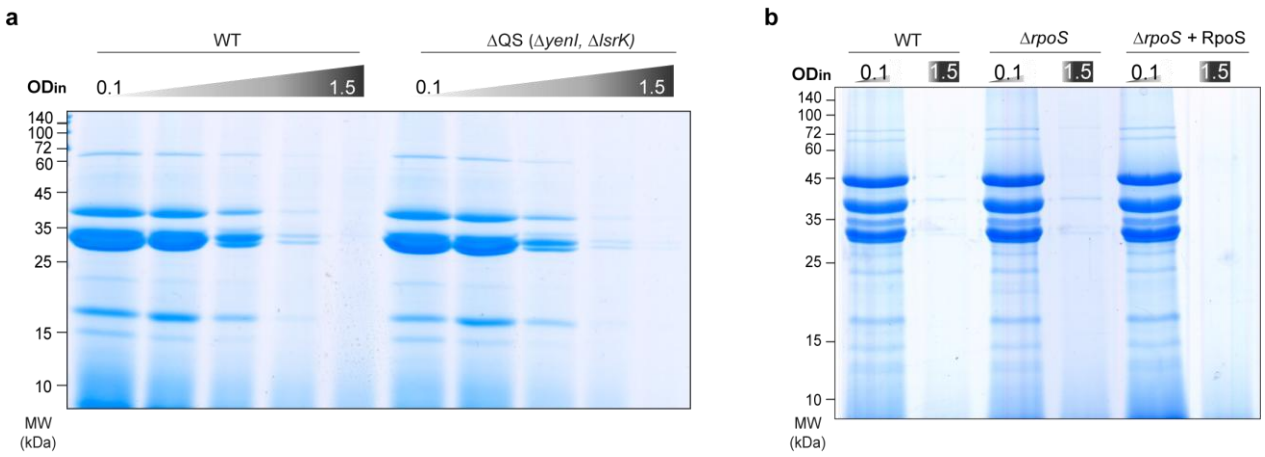

193 **Fig. 4 – Quorum sensing and the alternative sigma factor RpoS do not significantly contribute to the density-**
194 **dependent downregulation of the T3SS.**

195 **a)** Secretion assay of wild-type (WT) and quorum sensing mutant strains at different OD_{in} as used in Fig. 1 (left
196 to right, OD_{in}=0.1, 0.3, 0.7, 1.0, 1.5). **b)** Secretion assay of the indicated strains at OD_{in} 0.1 and 1.5, as displayed.
197 For *in trans* complementation of the *rpoS* mutant from pBAD::RpoS, RpoS expression was induced by the
198 addition of 0.2% arabinose at the time of the shift to 37°C. *n*=3, gel images show representative results.

199

200 **The transcriptional regulator VirF is the main target of the density-dependent T3SS regulation**

201 Based on the specificity of the d^3T3 (Fig. 3a), the uniform influence on all T3SS components (Table 1, Suppl.
202 Fig. 6), and the limited role of the tested global regulators (Fig. 4, Suppl. Fig. 8), we hypothesized the target
203 of the repression to be a general regulator of the T3SS. Expression and assembly of the injectisome are
204 controlled mainly by the AraC-like transcriptional activator VirF (Suppl. Fig. 9a). In the absence of VirF, the
205 *Yersinia* T3SS is inactive and its components are strongly repressed [19,65,66] (Suppl. Fig. 9b). VirF was
206 among the proteins that were significantly downregulated at high cell densities (-12.64-fold, $p<10^{-5}$,
207 Table 1). To test if this downregulation is the causal factor for the d^3T3, we expressed VirF from a plasmid
208 at OD_{in}=1.5. Additional expression of VirF was indeed sufficient to restore T3SS activity (Fig. 5a), indicating
209 that T3SS repression at higher cell densities largely is a consequence of reduced VirF levels. Based on these
210 results, added VirF expression should lead to uniform T3SS activity in microcolonies. To test this, we
211 imaged a microcolony grown as previously (Fig. 1b), but formed by *Y. enterocolitica* expressing additional
212 VirF from plasmid. In line with this hypothesis, the resulting increase in VirF levels abolished the
213 downregulation of T3SS activity in the center of the colony, leading to a homogenously T3SS-active
214 microcolony (Fig. 5b, Suppl. Fig. 10).

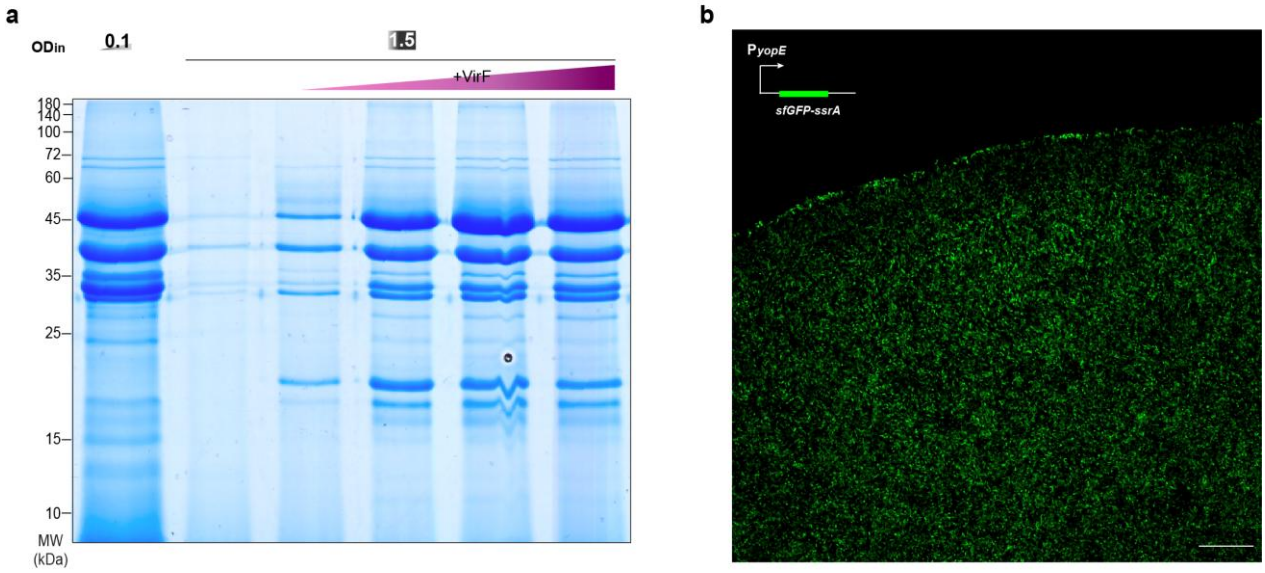

215

216 **Fig. 5 – Additional expression of the transcriptional regulator VirF at higher densities restores T3SS secretion.**
217 **a)** Secretion assay showing effector secretion at OD_{in}=0.1 (left) and 1.5 (right). Lanes 3-6, increasing expression
218 of VirF *in trans* (arabinose concentrations of 0.001, 0.003, 0.008, 0.03%, respectively). **b)** Confocal microscopy
219 image of a *Y. enterocolitica* Δ*sctW* P_{yopE}-*sfGFP-ssrA* microcolony additionally expressing VirF (induced by 0.2%
220 arabinose) at 37°C. T3SS activity, visualized by the sfGFP signal, is detected throughout the colony. Scale bar,
221 50 µm; *n*=3 for all panels, images display representative results.

222

223 **Bacterial density influences VirF levels at a post-transcriptional level via the CsrABC pathway**

224 We next investigated how cell density influences VirF levels. VirF is encoded in the *sctG-virF* operon
225 (Fig. 6a). *sctG* encodes the pilotin protein, which assists the assembly of the T3SS secretin ring in the OM
226 [67,68], but also has additional post-assembly functions [69]. Interestingly, it is the only T3SS component
227 whose expression is largely VirF-independent [18,19,70]. Total proteome analysis and immunoblots
228 showed SctG to be significantly less affected by higher cell densities than VirF or other T3SS components
229 (Fig. 6b, Suppl. Fig. 11, Table 1). Fluorescence microscopy confirmed this on a single-cell basis (Fig. 6c).
230 These results indicate that the regulatory region directly upstream of *virF*, rather than the promoter of the
231 *sctG-virF* operon, is the target of d^3T3. To discriminate between transcriptional and post-transcriptional
232 regulation, we measured the transcript abundance of *sctG* and *virF* by quantitative reverse transcription
233 polymerase chain reaction (RT-qPCR). Mirroring the expression data, *virF* transcript levels were more
234 strongly reduced at higher densities than *sctG*, pointing towards a cell density-driven post-transcriptional
235 targeting of the *virF* mRNA (Fig. 6d). A known regulator of *virF* transcript abundance is the CsrABC pathway.
236 In *Yersinia*, CsrA modulates T3SS activation via *virF* transcript regulation. CsrA binds to the *sctG-virF* mRNA
237 intergenic region as a dimer, stabilizing the *virF* transcript by reducing its turnover rate [55,71] (Fig. 6e).
238 The two conserved regulatory non-coding RNAs CsrB and CsrC (Suppl. Fig. 12) sequester CsrA, preventing
239 it from binding and stabilizing the *virF* transcript. To investigate a possible involvement of the CsrABC
240 system in the d^3T3, we measured CsrB and CsrC levels at different densities and observed a significant
241 upregulation of CsrB and especially CsrC at higher bacterial densities (Fig. 6f). As CsrA levels remain
242 relatively constant at the different bacterial densities (Suppl. Table 4), this suggests that the subsequent
243 increased sequestration of CsrA by CsrC underlies the *virF* downregulation that causes d^3T3 at higher
244 bacterial densities.

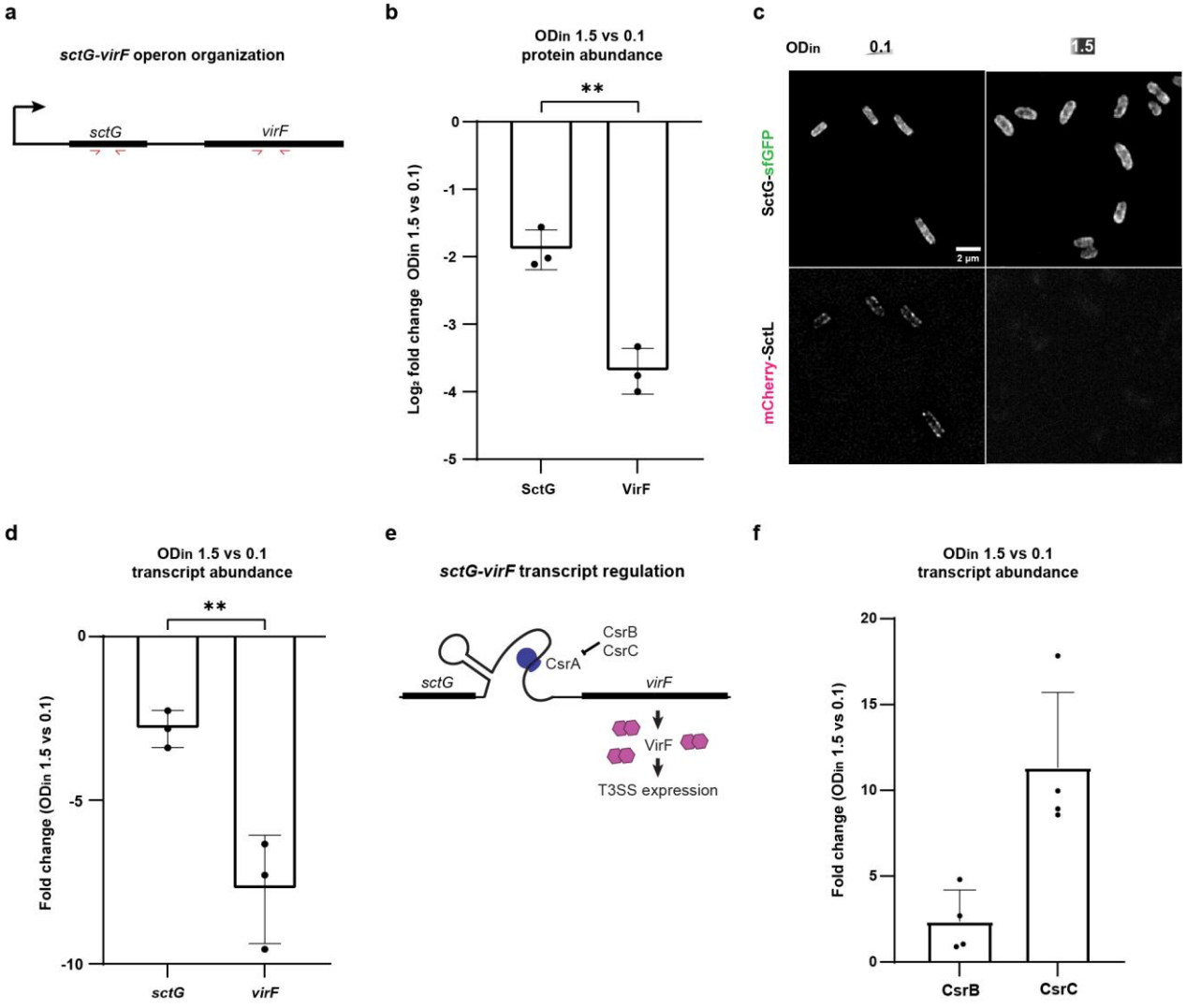

Fig. 6 – Bacterial density governs T3SS activity via posttranscriptional control of the *virF* transcript.

a) Organization of the *sctG-virF* operon, bold lines depict coding regions [18,69,72], red arrows indicate the position of RT-PCR primers. **b)** Protein levels of SctG and VirF at OD_{in} 1.5 vs. 0.1 (displayed as log_2 fold change), as measured by quantitative proteomics. **c)** Fluorescence microscopy of SctG-sfGFP (top) and the VirF-dependent T3SS component mCherry-SctL, both expressed from their native genetic background, at OD_{in} = 0.1 (left) or 1.5 (right). *n*=3, micrographs display representative results. **d)** Transcript levels of *sctG* and *virF* at OD_{in} 1.5 vs. 0.1, as measured by reverse transcriptase quantitative PCR (see panel A). **e)** Schematic depiction of the influence of the CsrABC system on VirF production [26,55,73]. The regulatory RNAs CsrB and CsrC sequester CsrA, preventing it from binding and stabilizing the *virF* transcript. Expression levels of the three components of the regulatory system are linked via feedback loop mechanisms [74] (see Suppl. Fig. 13). **f)** Transcript levels of CsrB and CsrC at OD_{in} 1.5 vs. 0.1, as measured by reverse transcriptase quantitative PCR. In b), d) and f), points indicate individual biological replicates, whiskers denote standard deviation. Statistical analysis was performed using a non-parametric t-test, **, $p<0.01$.

260 **Host-cell adhesion is affected by cell density**

261 Adhesion to host cells is a key virulence factor for many bacterial pathogens and a prerequisite for the
262 utilization of the T3SS. Accordingly, the trimeric *Yersinia* adhesin YadA, which is co-encoded with the T3SS
263 on the pYV virulence plasmid, is also regulated by VirF [75,76]. In line with this co-regulation, total
264 proteome analysis showed a strong downregulation of YadA at higher cell densities (OD_{in} 1.5) (31.3-fold,
265 $p<10^{-6}$) (Fig. 7a) – in fact, YadA is the only non-T3SS protein within the 25 proteins most affected by the
266 d^3T3 (Fig. 3a, Suppl. Fig. 6). To test whether this downregulation leads to a decreased adhesion to
267 eukaryotic cells, which might promote the detachment and dissemination of bacteria at higher cell
268 densities occurring at the later stages of infection, we performed an attachment assay to adherent HeLa
269 cells. Indeed, bacteria incubated at higher densities prior to the assay attached significantly less than the
270 reference (OD_{in}=0.1); the reduction almost mimicked the behavior of bacteria lacking *yadA*, which were
271 used as a control (Fig. 7b). These results indicate a coordinated downregulation of T3SS activity and
272 bacterial adhesion at higher densities.

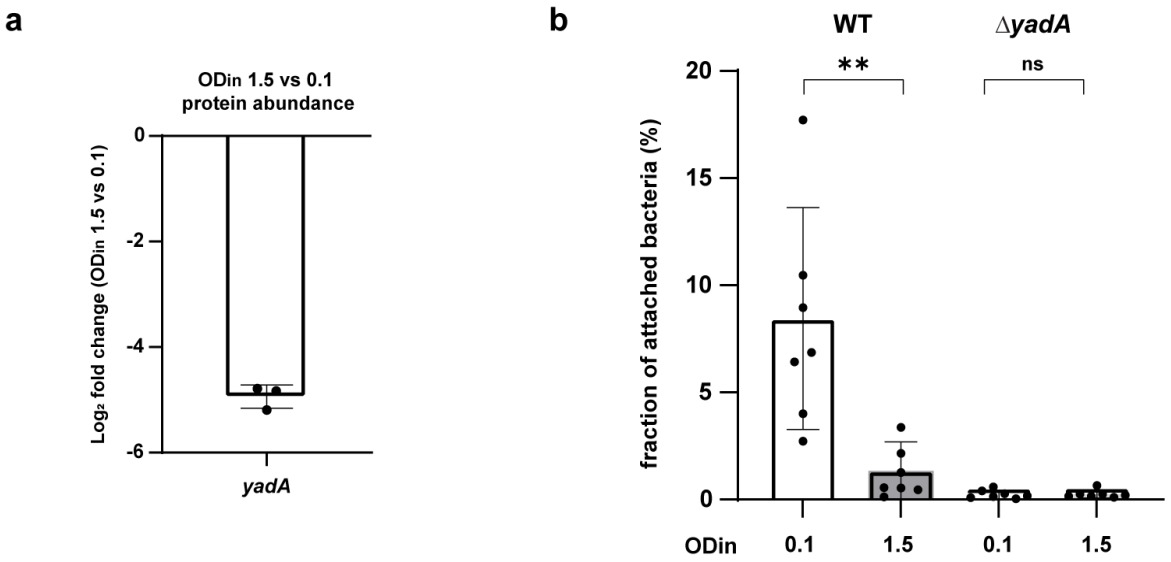

273

274 **Fig. 7 – Host-cell adhesion is significantly downregulated at higher cell densities.**
275 **a)** Protein levels of YadA at OD_{in} 1.5 vs. 0.1, as measured by quantitative proteomics. Points indicate individual
276 biological replicates, whiskers denote standard deviation. *n*=3. **b)** Attachment of wild-type (WT) or *ΔyadA*
277 bacteria to HeLa cells at the conditions indicated (OD_{in}=0.1, 1.5) (displayed as fraction of attached bacteria).
278 Points indicate individual biological replicates, whiskers denote standard deviation. Statistical analysis was
279 performed using a non-parametric t-test **, $p<0.01$, ns, $p>0.05$.

280

281 **Discussion**

282 To establish an infection, bacterial pathogens initially need to enter the host organism and defend
283 themselves against the host immune system on the way to their replication niches. However, after this
284 initiation of infection, it is equally important for the bacteria to propagate in their niches and disseminate
285 to other areas of the host organism or other hosts, steps that are often less appreciated and understood.
286 The T3SS is a major virulence factor for important bacterial pathogens including *Salmonella*, *Shigella*,
287 *Yersinia* and pathogenic *E. coli*. Its role in the establishment of infections is well-characterized and includes
288 bacterial uptake and the establishment of inflammation in *Salmonella* [77], inhibition of phagocytosis and
289 inflammation in *Yersinia* and *Shigella* [78,79], and actin pedestal formation and colonization in pathogenic
290 *E. coli* [80]. However, presence of the T3SS may become an obstacle in the later steps of infection, because
291 T3SS activity severely restricts bacterial growth and division across main T3SS model organisms, including
292 *Yersinia* [26,27], *Salmonella* [32], and *Shigella* [34,81]. In this study, we set out to address this important
293 conundrum by investigating the formation and activity of the *Y. enterocolitica* T3SS during microcolony
294 formation. We found that *Yersinia* selectively activates T3SS expression and assembly only in cells at the
295 rim of the microcolony. The phenotype can be explained by an active downregulation of the system at
296 higher local densities, which we characterized in liquid cultures at controlled growth conditions. Our
297 findings contrast with the previous picture of a completely T3SS-positive *Yersinia* population obtained
298 from studies that focused on the initiation of an infection and therefore used lower cell densities
299 [42,45,47,48,55,77]. Proteome analysis showed that the density-dependent T3SS downregulation is a
300 highly specific phenotype that affects all T3SS components and the coregulated adhesion factor YadA, but
301 very few non-T3SS-associated proteins (Fig. 3a, Table 1, Suppl. Fig. 6, Suppl. Table 2).

302 We found that the density-dependent downregulation of the T3SS is mediated by a pathway involving
303 CsrABC and VirF, the main T3SS transcription factor in *Yersinia*. At higher bacterial densities, higher
304 concentrations of the regulatory RNAs CsrB and CsrC sequester the regulatory protein CsrA, which usually
305 stabilizes the *virF* transcript [55,71] (Fig. 8b). This leads to a gradual inhibition of the expression of VirF
306 and, subsequently, all T3SS components, preventing the formation of injectisomes and protein secretion
307 by the T3SS. The post-transcriptional nature of the effect of the CsrABC system on VirF [78] is illustrated
308 by the finding that while *sctG* transcript levels are reduced at higher bacterial densities, this is most likely
309 a secondary effect of *virF* transcript destabilization, as the effect on *virF* levels is significantly stronger
310 (Fig. 6b). This regulatory pathway is a main factor in the density-dependent downregulation of the T3SS,
311 which is highlighted by the finding that additional expression of VirF *in trans* restores T3SS activity at higher
312 bacterial densities and leads to homogenously T3SS-active microcolonies.

313 The CsrABC (carbon storage regulator) system, originally identified as a glycogen synthesis regulator in
314 *E. coli* [79] (Suppl. Fig. 13), acts as a general regulator of bacterial virulence, motility, quorum sensing and
315 biofilm formation via target mRNA transcript binding in many bacterial species [80–82]. Studies in

316 *Y. pseudotuberculosis* showed that the CsrABC system, which is regulated by complex feedback loops [74],
317 strongly affects expression of the T3SS [26,55,73]. Similar to previous studies of CsrABC-based regulation
318 of bacterial virulence, the precise upstream factors that convey the local bacterial density to the regulatory
319 RNAs remain unclear. We experimentally tested the involvement of several candidates, namely stringent
320 response, quorum sensing (QS), the alternative sigma factor RpoS, and factors secreted into or depleted
321 from the medium. There are several known links between QS and the T3SS, such as the inhibitory role of
322 cell-cell communication on *Vibrio harveyi* and *P. aeruginosa* T3SS at high cell density [83,84]. Furthermore,
323 Atkinson and colleagues provided evidence for a negative influence of QS on T3SS secretion in
324 *Y. pseudotuberculosis* during biofilm formation in *Caenorhabditis elegans* [85]. However, we found that a
325 *Y. enterocolitica* strain lacking functionality of both known QS systems still retained the d^3T3 (Fig. 4a). This
326 lack of influence of the QS on d^3T3 is in line with previous studies showing no effect of QS on
327 *Y. enterocolitica* T3SS regulation [56,58]. Similarly, we neither observed a significant downregulation of
328 T3SS activity in spent medium previously incubated at higher densities, nor a recovery of activity at high
329 densities upon provision of fresh medium (Fig. 3bc), showing that any potential factor in the medium that
330 might control T3SS activity would be short-lived.

331 The T3SS is an essential virulence factor for many of the pathogenic bacteria that employ it, such as
332 *Salmonella*, *Shigella* and *Yersinia*. However, its presence and activity are a double-edged sword: While the
333 T3SS allows to manipulate host cells and in this way to evade the immune response (reviewed in [86]), or
334 to ensure the bacterial entry into target cells (reviewed in [87]), its activity severely restricts the bacterial
335 ability to multiply. Accordingly, assembly and activity of the T3SS are tightly regulated. A striking example
336 is the regulated expression of the SPI-1 T3SS in *Salmonella enterica*, where the inflammation caused by
337 the activity of the T3SS in a fraction of bacteria leads to a clearing of bacterial competitors, allowing the
338 T3SS-negative siblings to fill the resulting niche [34,88,89]. A similar effect was previously not observed for
339 *Yersinia*, which is uniformly T3SS-positive at the low densities used for most laboratory experiments
340 [42,47,48,55]. This could be rationalized by the fact that, like in *Shigella*, the T3SS mainly provides an
341 individual advantage by phagocytosis and inflammation inhibition [77,90,91]. However, like other bacteria,
342 *Yersinia* needs to propagate in its niche. We hypothesize that the d^3T3, described in this study, allows
343 efficient bacterial replication in colonized niches and the subsequent spreading from these niches and
344 microcolonies. Mouse infection experiments confirmed that bacterial densities in several organs steeply
345 rise at later stages of infection (e.g. by about 100-fold between day 2 and day 5 [92]) and the formation of
346 microcolonies in the liver and spleen of infected mice [93,94], suggesting that this phenotype may be
347 relevant during infection. Our results partially contrast with the more uniform YopE expression (measured
348 as YopE-mCherry signal) that was previously shown for *Y. pseudotuberculosis* microcolonies exposed to
349 innate immune system cells [93]. A possible reason for this discrepancy is the higher temporal resolution
350 of the reporter system used in our study (P_{yopE}-*sfGFP-ssrA*, Suppl. Fig. 1), which also does not interfere with
351 secretion, as has been shown for fusions of full-length T3SS effectors to fluorescent proteins [95]. The

352 complete downregulation of expression and assembly of the T3SS components shown in our experiments
353 further ensures that the T3SS cannot be unspecifically activated upon contact to eukaryotic cells during
354 this later phase of the infection and especially during dissemination.

355 A key aspect of the d^3T3 is that besides all components of the T3SS, it also affects YadA, a trimeric
356 autotransporter adhesin mediating the adhesion to extracellular matrix components of eukaryotic host
357 cells [75,76,96] which is also part of the VirF regulon. As shown in Fig. 7, this downregulation has a striking
358 effect on bacterial attachment not only to each other, but also to eukaryotic cells, allowing bacteria to
359 detach from eukaryotic cells, possibly leading to the disintegration of the microcolonies, and preventing
360 reattachment during dissemination. YadA has a highly pleiotropic role during infection, leading to diverse
361 outcomes across *Yersinia* species. It is essential for virulence in *Y. enterocolitica*, dispensable in
362 *Y. pseudotuberculosis*, and detrimental if expressed in *Y. pestis*. In *Y. enterocolitica*, YadA contributes to
363 serum resistance and exhibits a primarily antiphagocytic effect in synergy with the T3SS [75,76]. The
364 antiphagocytic function of YadA is largely attributed to its role in mediating tight adhesion of
365 *Y. enterocolitica* to macrophages, facilitating T3SS activation and the injection of antiphagocytic effectors.
366 Additionally, YadA promotes autoagglutination and microabscess formation, further hindering
367 phagocytosis. The density-dependent downregulation of adhesion and type III secretion described in this
368 manuscript is therefore likely to render the disseminating bacteria more vulnerable to phagocytosis. This
369 raises the intriguing possibility that the density-dependent T3SS downregulation synchronizes bacterial
370 dissemination as a strategy to optimize infection dynamics. Importantly, the reversibility of the d^3T3
371 (Fig. 3b) ensures that once bacteria are in a site with a lower local bacterial concentration, the T3SS can be
372 reassembled, a process that takes 30-60 minutes [44], sufficient to disseminate in or between hosts, but
373 ensuring that the T3SS is ready for the establishment of a fresh infection cycle at the new site.

374 In summary, we show that contrary to what was previously believed, *Y. enterocolitica* downregulates the
375 expression of its T3SS and the associated adhesin YadA at higher bacterial densities, such as inside
376 microcolonies. This specific downregulation is conveyed by the CsrABC system via the main T3SS
377 transcription factor VirF: Increased levels of the regulatory RNAs CsrB and especially CsrC at higher local
378 densities sequester CsrA and thereby destabilize the *virF* transcript. The resulting T3SS- and YadA-negative
379 population can multiply and disseminate, even in the presence of potential target cells, an important
380 aspect of bacterial virulence (Fig. 8). Future experiments may reveal whether similar mechanisms ensure
381 efficient replication and dissemination of *Shigella* and other T3SS-utilizing pathogens.

382

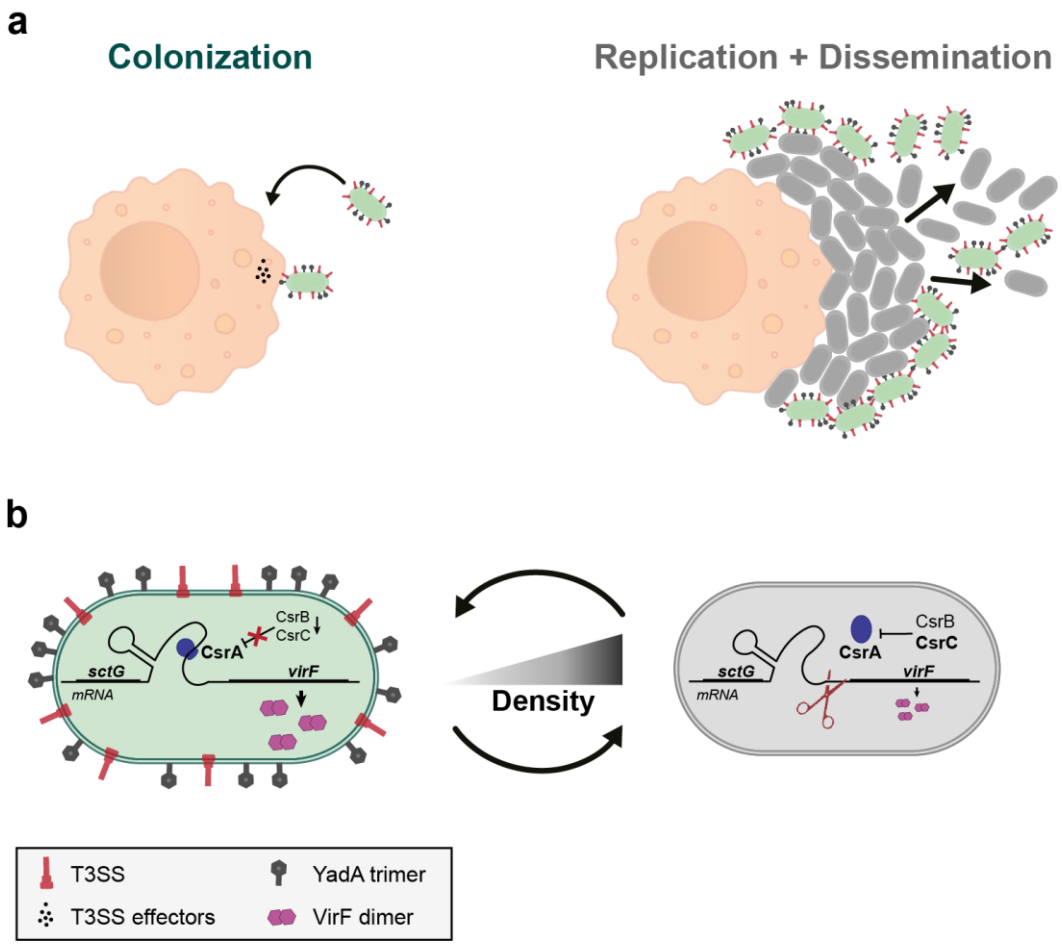

Fig. 8 – Influence of local higher cell density on T3SS secretion and on host-cell attachment.

a) At lower cell densities (left), *Yersinia* relies on the adhesion protein YadA (depicted in grey on the bacterial surface) and effector secretion by the T3SS (depicted in red on the bacterial surface) to colonize the host by fighting the host immune system. In a microcolony, where higher cell densities are perceived (right), *Yersinia* specifically downregulates T3SS secretion and YadA adhesion to efficiently replicate and ultimately spread and disseminate. **b)** Both adhesion and secretion are regulated by the transcription factor VirF. Upon host entry, sensed as 37°C shift, the *virF* transcript is stabilized thanks to the global mRNA regulator CsrA. The efficient binding of CsrA to *virF* mRNA and resulting expression of T3SS components are ensured by the low basal levels of the two CsrA inhibitory RNAs CsrBC [26,55,73]. At higher local cell densities, increased CsrC levels sequester CsrA, which causes a higher turnover of the *virF* transcript, leading to a decreased expression of T3SS components and YadA. The resulting decrease in adhesion and T3SS activity promotes *Yersinia* replication and dissemination at later stages of infection.

397 **Materials & Methods**

398 **Bacterial strain generation and genetic constructs**

399 A list of strains and plasmids used in this study can be found in Suppl. Table 5. The *Y. enterocolitica* strains
400 used in this study are based on the *Y. enterocolitica* wild-type strain MRS40 or its derivate IML421asd
401 (ΔHOPEMTasd). IML421asd lacks the major virulence effector proteins (YopH,O,P,E,M,T) and harbors a
402 deletion in the aspartate-beta-semialdehyde dehydrogenase gene, making the strain auxotrophic for
403 diaminopimelic acid (DAP) and therefore suitable for work in a biosafety class 1 environment [97].

404 **Bacterial cultivation, secretion assay, and total protein assays**

405 *Y. enterocolitica* overnight cultures were grown on a shaking incubator at 28°C in brain heart infusion
406 medium (BHI) supplemented with nalidixic acid (Nal, 35 µg/ml) and DAP (60 µg/ml), where required. Day
407 cultures (BHI supplemented with 35 µg/ml Nal, 60 µg/ml DAP where required, 20 mM $MgCl_2$, 0.4% glycerol,
408 and 5 mM EGTA for secreting conditions or 5 mM $CaCl_2$ for non-secreting conditions) were inoculated from
409 stationary overnight cultures (which typically were at an OD_{600} of 12-18) to an OD_{600} of 0.1, 0.3, 0.7, 1.0, or
410 1.5 by directly adding the required amount of the overnight culture to fresh medium. To select for the
411 maintenance of expression plasmids, 200 µg/ml ampicillin was added, where required. Day cultures were
412 incubated at 28°C for 90 min after the inoculum. Expression of the *yop* regulon was then induced by a
413 rapid temperature shift to 37°C. Where needed, protein expression from pBAD-His/B (Invitrogen)
414 derivative plasmids was induced at the temperature shift by adding 0.01–0.2% L-arabinose, as described
415 for the respective experiments. Unless specified otherwise, bacteria were incubated for 150-180 min after
416 the shift to 37°C. For secretion assays, 2 ml of the culture supernatant was harvested by centrifugation (10
417 min, 21,000 *g*) 180 min after the shift to 37°. Proteins in the supernatant were precipitated with 10%
418 trichloroacetic acid (TCA) at 4°C for 1-8 h. Precipitated proteins were collected by centrifugation (15 min,
419 21,000 *g*, 4°C). After washing with ice-cold acetone (1 ml), the pellets were resuspended in SDS-PAGE
420 loading buffer and normalized to 0.3 OD units (ODu)/15 µl for total cell analysis, or 0.6 ODu/15 µl for
421 secretion assays (1 ODu = 1 ml of culture at OD_{600} of 1, ~ 5 x 10^8 *Y. enterocolitica*). After resuspension,
422 samples were incubated for 5 min at 99°C and 15 µl were applied to SDS-PAGE analysis. Protein separation
423 was performed on 15% SDS-PAGE gels and protein sizes were determined using the BlueClassic Prestained
424 Marker (Jena Biosciences) as standard. For visualization, the gels were stained with FastGene-Q-stain
425 (NipponGenetics). Secretion efficiency was determined in Fiji [99] by gel densitometry for the YopH band,
426 compared to the wild-type strain. For immunoblots, the separated proteins were transferred to a
427 nitrocellulose membrane. Primary mouse anti-GFP antibody (ThermoFisher Proteintech 66002-1-Ig,
428 1:4000) was used in combination with a secondary anti-mouse antibody conjugated to horseradish
429 peroxidase (GE Healthcare NXA931, 1:5000). Primary rabbit anti-mCherry antibody (BioVision 5993
430 1:2000) was used in combination with a secondary anti-rabbit antibody conjugated to horseradish

431 peroxidase (Sigma-Aldrich A8275 1:10 000). For visualization, Immobilon Forte chemiluminescence
432 substrate (Sigma-Aldrich) was used in a LAS-4000 Luminescence Image Analyzer.

433

434 **Growth curve and promoter activity assays**

435 For growth curves and measurements of T3SS activation via upregulation of the YopE promoter (P*yopE-*
436 *sfGFP::ssrA*), bacteria were treated as described above. After 90 min at 28°C, bacterial cultures were
437 aliquoted in quadruplicates into a 96-well microplate (120 µl/well). sfGFP fluorescence (excitation: 480/25
438 nm, emission: 535/28 nm) for P*yopE* activity assays and absorbance at 600 nm for growth curves were
439 measured at 37°C over time in a Tecan Infinite 200 Pro photometer. The measured absorbance was
440 converted into OD_{600} based on a calibration performed using the same culture volume and microtiter plate
441 [98].

442 For sfGFP::ssrA degradation kinetics measurement, bacteria were treated as described before. After 120
443 min at 37°C in secreting-inducing conditions (5 mM EGTA), T3SS induction was stopped by adding 10 mM
444 Ca^{2+}. Bacterial cultures were aliquoted in quadruplicates into a 96-well microplate and sfGFP fluorescence
445 was measured as indicated above.

446 **Fluorescence Microscopy**

447 For fluorescence microscopy, bacteria were grown as described above. After 2.5 h at 37°C, 500 µl of culture
448 were harvested by centrifugation (2 min, 2400 *g*) and resuspended in 250 µl of microscopy medium (100
449 mM 2-[4-(2-Hydroxyethyl)piperazin-1-yl]ethane-1-sulfonic acid (HEPES) pH 7.2, 5 mM $(NH_4)_2SO_4$, 100 mM
450 NaCl, 20 mM sodium glutamate, 10 mM $MgCl_2$, 5 mM K_2SO_4, 50 mM 2-(N-morpholino) ethane sulfonic acid
451 (MES), 50 mM glycine). 2 µl of bacterial resuspension were spotted on an agarose pad (1.5% low melting
452 agarose (Sigma-Aldrich) in microscopy medium, 1% casamino acids, 5 mM EGTA) in a glass depression
453 slide (Marienfeld). For imaging, a Deltavision Elite Optical Sectioning Microscope equipped with a
454 UPlanSApo 100×/1.40 oil objective (Olympus) and an EDGE sCMOS_5.5 camera (Photometrics) was used.
455 z stacks with 9 slices (Δz = 0.15 µm) were acquired. The GFP signal was visualized using a FITC filter set
456 (excitation: 475/28 nm, emission: 535/48 nm) with 0.2 s exposure time. The mCherry signal was visualized
457 using a mCherry filter set (excitation: 575/25 nm, emission: 625/45 nm) with 0.2 s exposure time. Images
458 were processed with FIJI (ImageJ 1.51f/1.52i/1.52n) [99]. Fluorescence quantification was performed in
459 FIJI. For visualization purposes, selected fields of view adjusted identically for brightness and contrast
460 within the compared image sets are shown.

461 **Quantification of fluorescent foci**

462 To quantify the number of stable EGFP-SctQ foci, individual *Y. enterocolitica* cells were first segmented
463 using the neural network StarDist [100]. The training dataset was generated by manually annotating 17
464 images of *Y. enterocolitica* cells grown in BHI medium and imaged on agarose pads using the Deltavision

465 Elite Optical Sectioning Microscope. To account for variation in the imaging plane, z-stacks with 0.15 µm
466 spacing were recorded, of which 5 slices were selected for network training. The resulting 85 images were
467 quartered, resulting in a final dataset of 300 (training) and 40 (validation) image pairs. Dataset size was
468 increased 4-fold during training using flipping and rotation. The StarDist model was trained for 100 epochs
469 via the ZeroCostDL4Mic platform [101] using a batch size of 4, 260 steps, 120 rays, grid size of 2, an initial
470 learning rate of 0.0003 and an train/test split of 80%/20%. The dataset and model are included in the
471 DeepBacs [102] collection on Zenodo (doi: 10.5281/zenodo.11105050). Foci localization was performed
472 using the Fiji plugin ThunderSTORM [103]. Localizations were identified using 3rd order B-Spline filtering
473 and local maximum approximation with a peak intensity threshold of 4-fold standard deviation of the 1st
474 wavelet level. For sub-pixel localization, peaks were fitted with an integrated Gaussian in a fitting radius
475 of 3 pixels. Finally, localizations were filtered by PSF width (sigma < 600 nm) and images were rendered as
476 a scatter plot with a magnification of 1. This allows for foci counting by measuring the integrated intensity
477 within the ROIs of segmented cells. To ensure that the foci are located within the cell outlines, each ROI
478 was enlarged by 2 pixels with the help of a custom-written Fiji macro. A manual of the entire procedure is
479 provided as Supplementary File 1.

480 **Confocal microscopy imaging**

481 For imaging of *Y. enterocolitica* microcolonies, 1 µl of a stationary overnight culture was spotted on an LB
482 plate supplemented with NaI (35 µg/ml), DAP (60 µg/ml), glycerol (0.4%), and incubated at 28°C. For
483 additional VirF expression, plates were supplemented with ampicillin (200 µg/ml) and Arabinose (0.2%) to
484 ensure maintenance and induction of the expression plasmid. After 16 h, the plate was shifted to 37°C for
485 4 h. For colony imaging, colonies were deposited upside down in 8-well glass-bottom slides (µ-Slide, 8-well
486 glass bottom; Ibidi, Gräfelfing), embedded in 250 µl of 1% low melting agarose (Sigma-Aldrich
487 (Taufkirchen)). Confocal z-stacks were acquired on a Zeiss LSM-880 microscope, sfGFP-expressing cells
488 were excited using an argon laser at 488 nm, through an LD-LCI Plan Apochromat 25x 0.8 NA multi-
489 immersion objective, using water as immersion liquid. Fluorescence emission was collected in the 490–
490 579 nm range. The pixel size (0.15 µm) and the distance between optical slices (1.18 µm) were adjusted
491 according to the Nyquist criterion.

492 **Proteome analysis by shotgun proteomics-based mass spectrometry**

493 Strains were grown and prepared as described above. After 2.5 h at 37°C, cultures were normalized to an
494 OD_{600} of 0.5, and 2 ml were harvested by centrifugation at 9,391 *g* for 2 min. The cells were washed three
495 times with ice-cold phosphate-buffered saline (PBS) (8 g/l NaCl, 0.2 g/l KCl, 1.78 g/l Na_2HPO_4*2H2O, 0.24
496 g/l KH_2PO_4, pH 7.4) (15,000 *g*, 10 min, 4°C) and resuspended in 300 µl lysis buffer (2% sodium lauroyl
497 sarcosinate (SLS), 100 mM ammonium bicarbonate). Then samples were heated for 10 min at 90°C and
498 sonicated with a vial tweeter after heating. Proteins were reduced with 5 mM Tris(2-carboxyethyl)
499 phosphine (Thermo Fischer Scientific) at 90°C for 15 min and alkylated using 10 mM iodoacetamide (Sigma

500 Aldrich) for 30 min at 20°C in the dark. Proteins were precipitated with a 6-fold excess of ice cold acetone
501 and incubation for 2h at -20°C, followed by two methanol washing steps. Dried proteins were reconstituted
502 in 0.2% SLS and the amount of proteins was determined by bicinchoninic acid protein assay (Thermo
503 Scientific). For tryptic digestion, 50 µg protein was incubated in 0.5% SLS and 1 µg of trypsin (Serva) at 30°C
504 over night. After digestion, SLS was precipitated by adding a final concentration of 1.5% trifluoroacetic acid
505 (TFA, Thermo Fisher Scientific). Peptides were desalted by using C18 solid phase extraction cartridges
506 (Macherey-Nagel). Cartridges were prepared by adding acetonitrile (ACN), followed by equilibration with
507 0.1% TFA. Peptides were loaded on equilibrated cartridges, washed with 5% ACN and 0.1% TFA containing
508 buffer and finally eluted with 50% ACN and 0.1% TFA. Dried peptides were reconstituted in 0.1%
509 Trifluoroacetic acid and then analyzed using liquid-chromatography-mass spectrometry carried out on an
510 Exploris 480 instrument connected to an Ultimate 3000 RSLC nano and a nanospray flex ion source (all
511 Thermo Scientific). The following separating gradient was used: 94% solvent A (0.15% formic acid) and 6%
512 solvent B (99.85% acetonitrile, 0.15% formic acid) to 25% solvent B over 40 min, and an additional increase
513 of solvent B to 35% for 20 min at a flow rate of 300 nl/min. MS raw data was acquired on an Exploris 480
514 (Thermo Scientific) in data independent acquisition (DIA) mode with a method adopted from [104]. The
515 funnel RF level was set to 40. For DIA experiments full MS resolutions were set to 120.000 at m/z 200 and
516 full MS, AGC (Automatic Gain Control) target was 300% with an IT of 50 ms. Mass range was set to 350–
517 1400. AGC target value for fragment spectra was set at 3000%. 45 windows of 14 Da were used with an
518 overlap of 1 Da. Resolution was set to 15,000 and IT to 22 ms. Stepped HCD collision energy of 25, 27.5,
519 30% was used. MS1 data was acquired in profile, MS2 DIA data in centroid mode. Analysis of DIA data was
520 performed using the DIA-NN version 1.8 [105] using a *Y. enterocolitica* GenBank protein database
521 (https://www.ncbi.nlm.nih.gov/nuccore/NZ_CP011286.1) to generate a dataset-specific spectral library
522 for the DIA analysis. The neural network based DIA-NN suite performed noise interference correction
523 (mass correction, RT prediction and precursor/fragment co-elution correlation) and peptide precursor
524 signal extraction of the DIA-NN raw data. The following parameters were used: Full tryptic digest was
525 allowed with two missed cleavage sites, and oxidized methionine and carbamidomethylated cysteine
526 residues. Match between runs and remove likely interferences were enabled. The precursor FDR was set
527 to 1%. The neural network classifier was set to the single-pass mode, and protein inference was based on
528 genes. Quantification strategy was set to any LC (high accuracy). Cross-run normalization was set to RT-
529 dependent. Library generation was set to smart profiling. DIA-NN outputs were further evaluated using
530 the SafeQuant [106,107] script modified to process DIA-NN outputs. The mass spectrometry proteomics
531 data have been deposited to the ProteomeXchange Consortium via the PRIDE partner repository with the
532 dataset identifier PXD052013 (reviewer access with username 'reviewer_pxd052013@ebi.ac.uk' and
533 password 'D1OJfvZp').

534 **Sequence analysis**

535 The CsrB and CsrC genetic regions of *Y. enterocolitica* KNG22703 (GenBank: CP011286.1) and
536 *Y. pseudotuberculosis* YPIII (NZ_CP009792.1) [108] were compared. Alignments based on nucleotide
537 sequence were performed by Clustal Omega.

538 **RT-qPCR**

539 Total RNA from *Y. enterocolitica* cells grown as described above was extracted using the Monarch Total
540 RNA Miniprep Kit (New England Biolabs). A 10^9 cells pellet was first washed with 1 ml cold resuspension
541 buffer (10 mM Tris-HCl pH 8.0, 100 mM NaCl, 1 mM EDTA) and resuspended in 250 µl cold resuspension
542 buffer. 250 µl of lysis buffer (50 mM Tris/HCl pH 8.0, 8% Sucrose, 1% Triton X-100, 10 mM EDTA, 0.4%
543 lysozyme) and 800 µl of Monarch Total RNA Miniprep Kit protectant buffer were added to the
544 resuspension and incubated for 30 min at 4°C. After incubation, the cell suspension was incubated at 72°C
545 for 15 min. RNA purification was performed according to the manufacturer´s protocol. DNase treatment
546 was performed using Turbo DNase (Thermo Fisher Scientific), followed by enzyme removal via Monarch
547 RNA Cleanup Kit (New England Biolabs). cDNA was generated from 1 µg RNA using LunaScript RT SuperMix
548 Kit (New England Biolabs). qPCR reactions were performed on an Applied Biosystems 7500 Real-Time PCR
549 system using the Luna Universal qPCR MasterMix (New England Biolabs) and the primers listed in Suppl.
550 Table 6. The DNA gyrase subunit *gyrB* was used as an internal control [109]. Data analysis was performed
551 using the comparative threshold cycle (C_T) method [110].

552 **Attachment assay**

553 In preparation for the cell adhesion assay, HeLa cells were seeded and grown overnight in individual wells
554 of 24-well cell culture plates (Grainer). Cells were incubated with fresh RPMI medium supplemented with
555 DAP (60 µg/ml) before the addition of bacteria. After 2h in secretion-inducing conditions (37°C, 5 mM
556 EGTA), approximately 5 x 10^6 bacteria were added to the PBS-washed HeLa monolayer (multiplicity of
557 infection ~ 20) and incubated for 45 min. The attached cells were washed three times after incubation.
558 HeLa cells and attached bacteria were collected via trypsinization and plated on *Yersinia* selective plates
559 containing nalidixic acid (35 µg/ml) and DAP (60 µg/ml). After 24 h of incubation at 28°C, the number of
560 colony-forming units was calculated per each condition tested.

561

562 **Table 1 – Density-dependent regulation of expression of T3SS components.**

563 Label-free quantitative mass spectrometry of T3SS components in the total proteome of a ΔHOPEMTasd wild-
564 type strain at the different growth conditions indicated. Proteins are sorted by the ratio of intensity at OD_{in}
565 1.5/OD_{in} 0.1 (red shades: downregulated at OD_{in} 1.5, blue shades: upregulated at OD_{in} 1.5), which the *p* values
566 refer to as well. Exp.app., IM export apparatus; # pept., number of total detected peptides. Note that for some
567 effectors, the mutations in the ΔHOPEMTasd strain allow the detection of a subset of peptides (see Suppl. Table
568 5 for details). *n.d.*, not detected; imputed values were used for the statistical analysis in these cases.

Protein	Log_2 intensity ratio	*p* value	Individual log_2 intensity values						# pept.
			OD_{in} = 0.1			OD_{in} = 1.5			
Rod / washer SctI	-8.00	6.9E-08	27.30	27.79	27.78	19.42	19.56	19.89	10
Unknown T3SS-associated (ORF91A)	-7.64	1.6E-07	28.80	28.80	28.90	21.05	20.71	21.54	10
IM ring component SctD	-6.29	2.4E-05	29.83	29.83	29.89	22.59	23.72	24.38	20
Exp.app. component SctV	-6.24	2.3E-05	31.26	31.23	31.34	24.29	24.81	26.01	76
Exp.app. component SctR	-5.93	4.6E-07	25.81	25.83	25.98	*n.d.*	*n.d.*	*n.d.*	5
Effector YopO	-5.84	6.4E-06	31.16	31.23	31.24	24.63	25.83	25.65	25
Chaperone SycO	-5.64	9.1E-07	30.23	30.27	30.26	24.65	24.99	25.44	14
Translocator SctE (YopB)	-5.53	5.3E-06	33.23	33.97	33.42	27.54	28.04	28.44	39
Needle subunit SctF	-5.20	5.4E-08	30.92	30.91	30.93	25.68	25.52	25.96	13
Translocator SctA (LcrV)	-4.80	4.1E-07	33.40	33.35	33.39	28.29	28.56	28.90	58
Secretin / OM ring SctC	-4.66	2.6E-07	30.90	30.97	30.98	26.02	26.30	26.56	38
Regulator YscX	-4.59	5.4E-07	27.99	28.17	28.01	23.18	23.45	23.77	12
IM ring component SctJ	-4.59	9.2E-07	31.26	31.25	31.32	26.46	26.52	27.09	35
Chaperone YscE	-4.56	6.8E-09	29.74	29.73	29.92	25.25	25.17	25.29	13
Translocator SctB (YopD)	-4.54	7.4E-06	32.14	32.94	32.27	27.69	27.81	28.23	71
Chaperone YscB	-4.52	9.5E-07	30.65	30.60	30.78	25.83	26.15	26.49	13
Effector YopT	-4.48	7.4E-03	23.29	23.33	23.28	*n.d.*	16.56	*n.d.*	5
Chaperone YscG	-4.46	1.7E-07	29.24	29.19	29.29	24.59	24.70	25.04	8
Regulator LcrG	-4.25	1.9E-06	30.42	30.40	30.47	25.80	26.20	26.53	28
Chaperone SycT	-4.25	4.0E-07	24.33	23.33	23.41	*n.d.*	*n.d.*	*n.d.*	3
Cytosolic component SctK	-4.08	1.2E-06	28.67	28.68	28.75	24.39	24.58	24.90	18
Lipoprotein YlpA	-3.98	1.6E-06	30.97	30.94	30.90	26.89	27.28	27.50	21
Exp.app. component SctU	-3.94	2.4E-07	26.93	27.02	27.09	22.81	23.02	23.40	16
Cytosolic component SctL	-3.94	8.1E-07	29.00	29.06	29.12	24.90	25.13	25.33	16
Regulator YscY	-3.92	2.1E-06	26.31	26.29	26.40	22.55	22.09	22.60	5
Chaperone SycD	-3.87	1.6E-06	32.33	32.35	32.34	28.12	28.48	28.80	22
Transcriptional activator VirF (LcrF)	-3.70	4.7E-06	28.76	28.79	28.85	24.76	25.03	25.51	15
Cytosolic ATPase SctN	-3.56	1.1E-05	30.93	30.93	31.02	26.92	27.53	27.76	46
Effector YopQ	-3.54	1.3E-06	29.25	29.44	29.11	25.51	25.69	25.97	17
Chaperone SycN	-3.34	1.8E-07	29.71	29.65	29.97	26.39	26.42	26.51	9
Unknown T3SS-associated (ORF181)	-3.27	1.0E-08	25.65	25.60	25.70	22.87	22.86	22.80	8
Gatekeeper TyeA	-3.11	3.4E-08	29.16	29.16	29.20	25.99	26.02	26.19	9
Secreted protein YscH/YopR	-2.98	9.7E-07	27.09	27.10	26.92	24.00	23.88	24.27	5
Effector YopE	-2.47	5.2E-04	24.95	24.83	25.09	22.73	21.76	22.96	6
Needle length regulator / ruler SctP	-2.40	2.3E-05	30.30	30.37	30.36	27.59	27.97	28.26	45
Cytosolic component SctO	-2.30	1.4E-04	25.40	25.39	25.39	22.63	23.10	23.55	9
Regulator LcrR	-2.27	5.2E-07	27.41	27.43	27.55	25.11	25.14	25.33	6
Chaperone SycE	-2.10	4.5E-06	30.09	30.15	30.11	27.84	27.96	28.25	8

Exp.app. component SctT	-2.09	1.5E-02	22.65	22.34	22.24	*n.d.*	*n.d.*	*n.d.*	4
Cytosolic component SctQ	-2.06	1.1E-04	29.58	29.58	29.63	27.10	27.71	27.82	13
Pilotin SctG (YscW)	-1.90	2.4E-05	28.46	28.44	28.39	26.35	26.41	26.83	9
Secreted gatekeeper SctW (YopN)	-1.73	3.8E-04	30.68	31.00	30.70	28.66	29.10	29.42	25
Chaperone SycH	-0.02	7.4E-01	29.65	29.63	29.66	29.57	29.55	29.75	21
Secreted neg. regulator YscM1	0.81	1.4E-02	27.53	27.52	26.86	28.34	28.06	27.93	11
Secreted neg. regulator YscM2	2.36	1.1E-05	26.01	26.07	25.96	28.64	28.40	28.09	9

569

570 **References**

571

572 [1] Cornelis G. The type III secretion injectisome. Nat Rev Microbiol 2006.

573 [2] Deng W, Marshall NC, Rowland JL, McCoy JM, Worrall LJ, Santos AS, et al. Assembly, structure,
574 function and regulation of type III secretion systems. Nat Rev Microbiol 2017;15:323–37.

575 [3] Galán JE, Wolf-Watz H. Protein delivery into eukaryotic cells by type III secretion machines.
576 Nature 2006;444:567–73.

577 [4] Wagner S, Grin I, Malmsheimer S, Singh N, Torres-Vargas CE, Westerhausen S. Bacterial type III
578 secretion systems: A complex device for the delivery of bacterial effector proteins into eukaryotic
579 host cells. FEMS Microbiol Lett 2018;365.

580 [5] Bastedo DP, Lo T, Laflamme B, Desveaux D, Guttman DS. Diversity and evolution of type III
581 secreted effectors: A case study of three families. Curr Top Microbiol Immunol, vol. 427, Springer
582 Science and Business Media Deutschland GmbH; 2020, p. 201–30.

583 [6] Büttner D. Protein Export According to Schedule: Architecture, Assembly, and Regulation of Type
584 III Secretion Systems from Plant- and Animal-Pathogenic Bacteria. Microbiology and Molecular
585 Biology Reviews 2012;76:262–310.

586 [7] Jennings E, Thurston TLM, Holden DW. Salmonella SPI-2 Type III Secretion System Effectors:
587 Molecular Mechanisms And Physiological Consequences. Cell Host Microbe 2017;22:217–31.

588 [8] Hüsing S, Halte M, van Look U, Guse A, Gálvez EJC, Charpentier E, et al. Control of membrane
589 barrier during bacterial type-III protein secretion. Nat Commun 2021;12:3999.

590 [9] Kuhlen L, Abrusci P, Johnson S, Gault J, Deme J, Caesar J, et al. Structure of the core of the type iii
591 secretion system export apparatus. Nat Struct Mol Biol 2018;25:583–90.

592 [10] Berger C, Ravelli RBG, López-Iglesias C, Kudryashev M, Diepold A, Peters PJ. Structure of the
593 Yersinia injectisome in intracellular host cell phagosomes revealed by cryo FIB electron
594 tomography. J Struct Biol 2021;213.

595 [11] Butan C, Lara-Tejero M, Li W, Liu J, Galán JE. High-resolution view of the type III secretion export
596 apparatus in situ reveals membrane remodeling and a secretion pathway. PNAS 2019;12:24786–
597 95.

598 [12] Hu B, Morado DR, Margolin W, Rohde JR, Arizmendi O, Picking WL, et al. Visualization of the type
599 III secretion sorting platform of Shigella flexneri. Proc Natl Acad Sci U S A 2015;112:1047–52.

600 [13] Hu B, Lara-Tejero M, Kong Q, Galán JE, Liu J. In Situ Molecular Architecture of the Salmonella Type
601 III Secretion Machine. Cell 2017;168:1065-1074.e10.

602 [14] Makino F, Shen D, Kajimura N, Kawamoto A, Pissaridou P, Oswin H, et al. The Architecture of the
603 Cytoplasmic Region of Type III Secretion Systems. Sci Rep 2016;6.

604 [15] Diepold A, Kudryashev M, Delalez NJ, Berry RM, Armitage JP. Composition, Formation, and
605 Regulation of the Cytosolic C-ring, a Dynamic Component of the Type III Secretion Injectisome.
606 PLoS Biol 2015;13:e1002039.

607 [16] Diepold A, Sezgin E, Huseyin M, Mortimer T, Eggeling C, Armitage JP. A dynamic and adaptive
608 network of cytosolic interactions governs protein export by the T3SS injectisome. Nat Commun
609 2017;8:15940.

610 [17] Wimmi S, Balinovic A, Brianceau C, Pintor K, Vielhauer J, Turkowyd B, et al. Cytosolic sorting
611 platform complexes shuttle type III secretion system effectors to the injectisome in Yersinia
612 enterocolitica. Nat Microbiol 2024;9:185–99.

613 [18] Böhme K, Steinmann R, Kortmann J, Seekircher S, Heroven AK. Concerted Actions of a Thermo-
614 labile Regulator and a Unique Intergenic RNA Thermosensor Control Yersinia Virulence. PLoS
615 Pathog 2012;8:1002518.

616 [19] Schwiesow L, Lam H, Dersch P, Auerbuch V. Yersinia Type III Secretion System Master Regulator
617 LcrF. J Bacteriol 2016;198:604.

618 [20] Forsberg, Viitanen A -M, Skurnik M, Wolf-Watz H. The surface-located YopN protein is involved in
619 calcium signal transduction in Yersinia pseudotuberculosis. Mol Microbiol 1991;5:977–86.

620 [21] Cheng LW, Kay O, Schneewind O. Regulated secretion of YopN by the type III machinery of
621 Yersinia enterocolitica. J Bacteriol 2001;183:5293–301.

622 [22] Cambronne ED, Schneewind O. Yersinia enterocolitica type III secretion: yscM1 and yscM2
623 regulate yop gene expression by a posttranscriptional mechanism that targets the 5' untranslated
624 region of yop mRNA. J Bacteriol 2002;184:5880–93.

625 [23] Stainier I, Cornelis GR. YscM1 and YscM2, two Yersinia enterocolitica proteins causing
626 downregulation of yop transcription. Mol Microbiol 1997.

627 [24] Allaoui A, Schulte R, Cornelis GR. Mutational analysis of the Yersinia enterocolitica virC operon:
628 characterization of yscE, F, G, I, J, K required for Yop secretion and yscH encoding YopR. Mol
629 Microbiol 1995;18:343–55.

630 [25] Kudryashev M, Diepold A, Amstutz M, Armitage JP, Stahlberg H, Cornelis GR. Yersinia
631 enterocolitica type III secretion injectisomes form regularly spaced clusters, which incorporate
632 new machines upon activation. Mol Microbiol 2015;95:875–84.

633 [26] Volk M, Vollmer I, Heroven AK, Dersch P. Transcriptional and Post-transcriptional Regulatory
634 Mechanisms Controlling Type III Secretion. Curr Top Microbiol Immunol 2020;427:11–33.

635 [27] Heroven AK, Böhme K, Dersch P. The Csr/Rsm system of Yersinia and related pathogens: a post-
636 transcriptional strategy for managing virulence. RNA Biol 2012;9:379–91.

637 [28] Kupferberg LL, Higuchi K. Role of calcium ions in the stimulation of growth of virulent strains of
638 Pasteurella pestis. J Bacteriol 1958;76:120–1.

639 [29] Fowler JM, Wulff CR, Straley SC, Brubaker RR, Robert Brubaker CR. Growth of calcium-blind
640 mutants of Yersinia pestis at 37 6C in permissive Ca 2+-deficient environments. Microbiology
641 (Reading) 2009.

642 [30] Ben-Gurion R, Shafferman A. Essential virulence determinants of different Yersinia species are
643 carried on a common plasmid. Plasmid 1981;5:183–7.

644 [31] Ferber DM, Brubaker RR. Plasmids in Yersinia pestis. Infect Immun 1981;31:839–41.

645 [32] Perry RD, Harmon PA, Bowmer WS, Straley SC. A Low-Ca2' Response Operon Encodes the V
646 Antigen of Yersinia pestis. Infect Immun 1986;54:428–34.

647 [33] Michiels T, Wattiau P, Brasseur R, Ruysschaert JM, Cornelis G. Secretion of Yop proteins by
648 yersiniae. Infect Immun 1990;58:2840–9.

649 [34] Sturm A, Heinemann M, Arnoldini M, Benecke A, Ackermann M, Benz M, et al. The cost of
650 virulence: Retarded growth of salmonella typhimurium cells expressing type iii secretion system
651 1. PLoS Pathog 2011;7.

652 [35] Carter PB, Zahorchak RJ, Brubaker RR. Plague Virulence Antigens from Yersinia enterocolitica. vol.
653 28. 1980.

654 [36] Sasakawa C, Kamata K, Sakai T, Murayama SY, Makino S, Yoshikawa M. Molecular Alteration of
655 the 140-Megadalton Plasmid Associated with Loss of Virulence and Congo Red Binding Activity in
656 Shigella flexneri. vol. 51. 1986.

657 [37] Milne-Davies B, Helbig C, Wimmi S, Cheng DWC, Paczia N, Diepold A. Life After Secretion—
658 Yersinia enterocolitica Rapidly Toggles Effector Secretion and Can Resume Cell Division in
659 Response to Changing External Conditions. Front Microbiol 2019;10:2128.

660 [38] Diard M, Garcia V, Maier L, Remus-Emsermann MNP, Regoes RR, Ackermann M, et al.
661 Stabilization of cooperative virulence by the expression of an avirulent phenotype. Nature
662 2013;494:353–6.

663 [39] Kroken AR, Chen CK, Evans DJ, Yahr TL, Fleiszig SMJ. The impact of ExoS on Pseudomonas
664 aeruginosa internalization by epithelial cells is independent of fleQ and correlates with bistability
665 of type three secretion system gene expression. MBio 2018;9:1–21.

666 [40] Lampaki D, Diepold A, Glatter T. A Serial Sample Processing Strategy with Improved Performance
667 for in-Depth Quantitative Analysis of Type III Secretion Events in Pseudomonas aeruginosa. J
668 Proteome Res 2020;19:543–53.

669 [41] Urbanowski ML, Brutinel ED, Yahr TL. Translocation of ExsE into Chinese hamster ovary cells is
670 required for transcriptional induction of the Pseudomonas aeruginosa type III secretion system.
671 Infect Immun 2007;75:4432–9.

672 [42] Wimmi S, Balinovic A, Jeckel H, Selinger L, Lampaki D, Eisemann E, et al. Dynamic relocalization of
673 cytosolic type III secretion system components prevents premature protein secretion at low
674 external pH. Nat Commun 2021;3:1625.

675 [43] Bajunaid W, Haidar-Ahmad N, Kottarampatel AH, Manigat FO, Silué N, Tchagang CF, et al. The t3ss
676 of shigella: Expression, structure, function, and role in vacuole escape. Microorganisms 2020;8:1–
677 28.

678 [44] Diepold A, Amstutz M, Abel S, Sorg I, Jenal U, Cornelis GR. Deciphering the assembly of the
679 Yersinia type III secretion injectisome. EMBO Journal 2010;29:1928–40.

680 [45] Milne-Davies B, Helbig C, Wimmi S, Cheng DWC, Paczia N, Diepold A. Life After Secretion—
681 Yersinia enterocolitica Rapidly Toggles Effector Secretion and Can Resume Cell Division in
682 Response to Changing External Conditions. Front Microbiol 2019;10.

683 [46] Burgess JL, Case HB, Burgess RA, Dickenson NE. Dominant negative effects by inactive Spa47
684 mutants inhibit T3SS function and Shigella virulence. PLoS One 2020;15.

685 [47] Wiley DJ, Rosqvist R, Schesser K. Induction of the Yersinia Type 3 Secretion System as an All-or-
686 None Phenomenon. J Mol Biol 2007;373:27–37.

687 [48] Cornelis G, Vanootegem J.-C, Sluiters C, Cornelis G. Transcription of the yop regulon from Y.
688 enterocolitica requires trans acting pYV and chromosomal genes. Microb Pathog 1987;2:367–79.

689 [49] Dewoody RS, Merritt PM, Marketon MM, Francis M, Forsberg A. Regulation of the Yersinia type III
690 secretion system: traffic control. Front Cell Infect Microbiol 2013.

691 [50] Jacobi CA, Roggenkamp A, Rakin A, Zumbihl R, Leitritz L, Heesemann J. In vitro and in vivo
692 expression studies of yopE from Yersinia enterocolitica using the gfp reporter gene. n.d.

693 [51] Farrell CM, Grossman AD, Sauer RT. Cytoplasmic degradation of ssrA-tagged proteins. Mol
694 Microbiol 2005;57:1750–61.

695 [52] Diepold A, Wagner S. Assembly of the bacterial type III secretion machinery. FEMS Microbiol Rev
696 2014;38:802–22.

697 [53] Hueck CJ. Type III Protein Secretion Systems in Bacterial Pathogens of Animals and Plants. vol. 62.
698 1998.

699 [54] Wagner S, Diepold A. A unified nomenclature for injectisome-type type III secretion systems. Curr
700 Top Microb Immunol, vol. 427, 2020, p. 1–10.

701 [55] Kusmierek M, Hoßmann J, Witte R, Opitz W, Vollmer I, Volk M. A bacterial secreted translocator
702 hijacks riboregulators to control type III secretion in response to host cell contact. PLoS Pathog
703 2019.

704 [56] Atkinson S, Sockett RE, Cámara M, Williams P. Quorum sensing and the lifestyle of Yersinia. vol. 8.
705 2006.

706 [57] Atkinson S, Chang C-Y, Sockett RE, Cámara M, Williams P. Quorum Sensing in Yersinia
707 enterocolitica Controls Swimming and Swarming Motility. J Bacteriol 2006;188:1451–61.

708 [58] Ng Y-K, Grasso M, Wright V, Garcia V, Williams P, Atkinson S. The Quorum Sensing System of
709 Yersinia enterocolitica 8081 Regulates Swimming Motility, Host Cell Attachment, and Virulence
710 Plasmid Maintenance. Genes (Basel) 2018.

711 [59] Badger JL, Miller VL. Role of RpoS in survival of Yersinia enterocolitica to a variety of
712 environmental stresses. J Bacteriol 1995;177:5370–3.

713 [60] Guan J, Xiao X, Xu S, Gao F, Wang J, Wang T, et al. Roles of RpoS in Yersinia pseudotuberculosis
714 stress survival, motility, biofilm formation and type VI secretion system expression. Journal of
715 Microbiology 2015;53:633–42.

716 [61] Brown A, Fernández IS, Gordiyenko Y, Ramakrishnan & V. Ribosome-dependent activation of
717 stringent control. Nature 2016;534.

718 [62] Wendrich TM, Blaha G, Wilson DN, Marahiel MA, Nierhaus KH. Dissection of the Mechanism for
719 the Stringent Factor RelA. vol. 10. 2002.

720 [63] Germain E, Guiraud P, Byrne D, Douzi B, Djendli M, Maisonneuve E. YtfK activates the stringent
721 response by triggering the alarmone synthetase SpoT in Escherichia coli. Nat Comm 2019.

722 [64] Traxler B, Beckwith J. Assembly of a hetero-oligomeric membrane protein complex. Proc Natl
723 Acad Sci U S A 1992;89:10852–6.

724 [65] Axler-Diperte GL, Stewart HJ, Wren BW, Darwin AJ. YtxR Acts as an Overriding Transcriptional Off
725 Switch for the Yersinia enterocolitica Ysc-Yop Type 3 Secretion System §. J Bacteriol
726 2009;191:514–24.

727 [66] Li L, Yan H, Feng L, Li Y, Lu P. LcrQ Blocks the Role of LcrF in Regulating the Ysc-Yop Type III
728 Secretion Genes in Yersinia pseudotuberculosis. PLoS One 2014;9:92243.

729 [67] Koster M, Bitter W, De Cock H, Allaoui AA, Cornelis GR, Tommassen J. The outer membrane
730 component, YscC, of the Yop secretion machinery of Yersinia enterocolitica forms a ring-shaped
731 multimeric complex. Mol Microbiol 1997.

732 [68] Rau R, Darwin AJ. Identification of YsaP, the pilotin of the Yersinia enterocolitica Ysa type III
733 secretion system. J Bacteriol 2015;197:2770–9.

734 [69] Wimmi S, Fleck M, Helbig C, Brianceau C, Langenfeld K, Szymanski WG, et al. Pilotins are mobile
735 T3SS components involved in assembly and substrate specificity of the bacterial type III secretion
736 system. Mol Microbiol 2024;2:304–23.

737 [70] Liu L, Huang S, Fei K, Zhou W, Chen S, Hu Y. Characterization of the binding motif for the T3SS
738 master regulator LcrF in Yersinia pseudotuberculosis. FEMS Microbiol Lett 2021;368:31.

739 [71] Ozturk G, Legrand K, Zheng Y, Young GM. Yersinia enterocolitica CsrA regulates expression of the
740 Ysa and Ysc type 3 secretion system in unique ways. FEMS Microbiol Lett 2017;364:204.

741 [72] Cornelis G, Sluiters C, Lambert de Rouvroit C, Michiels T. Homology between virF, the
742 transcriptional activator of the Yersinia virulence regulon, and AraC, the Escherichia coli arabinose
743 operon regulator. J Bacteriol 1989;171:254–62.

744 [73] Kusmierek M, Dersch P. Regulation of host-pathogen interactions via the post-transcriptional
745 Csr/Rsm system. Curr Opin Microbiol 2018;41:58–67.

746 [74] Pourciau C, Lai YJ, Gorelik M, Babitzke P, Romeo T. Diverse Mechanisms and Circuitry for Global
747 Regulation by the RNA-Binding Protein CsrA. Front Microbiol 2020;11:601352.

748 [75] El Tahir Y, Skurnik M. YadA, the multifaceted adhesin. Int J Med Microbiol 2001;8:209–18.

749 [76] Mühlenkamp M, Oberhettinger P, Leo JC, Linke D, Schütz MS. Yersinia adhesin A (YadA) - Beauty
750 & beast. International Journal of Medical Microbiology 2015;305:252–8.

751 [77] Milne-Davies B, Wimmi S, Diepold A. Adaptivity and dynamics in type III secretion systems. Mol
752 Microbiol 2021;115:395–411.

753 [78] Meyer I, Volk M, Salto I, Moesser T, Chaoprasid P, Herbrüggen AS, et al. RNase-mediated
754 reprogramming of Yersinia virulence. PLoS Pathog 2024;20:e1011965.

755 [79] Sabnis NA, Yang H, Romeo T. Pleiotropic Regulation of Central Carbohydrate Metabolism in
756 Escherichia coli via the Gene csrA. Journal of Biological Chemistry 1995;270:29096–104.

757 [80] Dubey AK, Baker CS, Romeo T, Babitzke P. RNA sequence and secondary structure participate in
758 high-affinity CsrA-RNA interaction. RNA 2005.

759 [81] Mercante J, Edwards AN, Dubey AK, Babitzke P, Romeo T. Molecular Geometry of CsrA (RsmA)
760 Binding to RNA and Its Implications for Regulated Expression. J Mol Biol 2009;392:511–28.

761 [82] Vakulskas CA, Potts AH, Babitzke P, Ahmer BMM, Romeo T. Regulation of Bacterial Virulence by
762 Csr (Rsm) Systems. Microbiology and Molecular Biology Reviews 2015;79:193–224.

763 [83] Darshanee Ruwandeepika HA, Karunasagar I, Bossier P, Defoirdt T. Expression and Quorum
764 Sensing Regulation of Type III Secretion System Genes of Vibrio harveyi during Infection of
765 Gnotobiotic Brine Shrimp. PLoS One 2015.

766 [84] Waters CM, Wu JT, Ramsey ME, Harris RC, Bassler BL. Control of the type 3 secretion system in
767 Vibrio harveyi by quorum sensing through repression of exsA. Appl Environ Microbiol
768 2010;76:4996–5004.

769 [85] Atkinson S, Goldstone RJ, Joshua GWP, Chang C-Y, Patrick HL. Biofilm Development on
770 Caenorhabditis elegans by Yersinia Is Facilitated by Quorum Sensing-Dependent Repression of
771 Type III Secretion. PLoS Pathog 2011;7:1001250.

772 [86] Cornelis GR. Mini-Review Yersinia type III secretion: send in the effectors. J Cell Biol
773 2002;158:401–8.

774 [87] Bajunaid W, Haidar-Ahmad N, Kottarampatel AH, Manigat FO, Silué N, Tchagang CF, et al.
775 microorganisms The T3SS of Shigella: Expression, Structure, Function, and Role in Vacuole Escape.
776 Microorganisms 2020.

777 [88] Ackermann M, Stecher B, Freed NE, Songhet P, Hardt W-D, Doebeli M. Self-destructive
778 cooperation mediated by phenotypic noise. Nature Letters 2008.

779 [89] Hautefort I, Proença MJ, Hinton JCD. Single-copy green fluorescent protein gene fusions allow
780 accurate measurement of Salmonella gene expression in vitro and during infection of mammalian
781 cells. Appl Environ Microbiol 2003;69:7480–91.

782 [90] Galán JE. Common Themes in the Design and Function of Bacterial Effectors. Cell Host Microbe
783 2009;5:571–9.

784 [91] Pha K. Yersinia type III effectors perturb host innate immune responses . World J Biol Chem
785 2016;7:1.

786 [92] Bent ZW, Branda SS, Young GM, Zachary Bent CW. The Yersinia enterocolitica Ysa type III
787 secretion system is expressed during infections both in vitro and in vivo. Microbiologyopen
788 2013;2:962–75.

789 [93] Davis KM, Mohammadi S, Isberg RR. Community behavior and spatial regulation within a bacterial
790 microcolony in deep tissue sites serves to protect against host attack. Cell Host Microbe 2015.

791 [94] Oellerich MF, Jacobi CA, Freund S, Niedung K, Bach A, Heesemann J, et al. Yersinia enterocolitica
792 infection of mice reveals clonal invasion and abscess formation. Infect Immun 2007;75:3802–11.

793 [95] Radics J, Königsmaier L, Marlovits TC. Structure of a pathogenic type 3 secretion system in action.
794 Nature Structural & Molecular Biology 2013 21:1 2013;21:82–7.

795 [96] Tertti R, Skurnik M, Vartio T, Kuusela P. Adhesion protein YadA of Yersinia species mediates
796 binding of bacteria to fibronectin. Infect Immun 1992;60:3021.

797 [97] Kudryashev M, Stenta M, Schmelz S, Amstutz M, Wiesand U, Castaño-Díez D, et al. In situ
798 structural analysis of the Yersinia enterocolitica injectisome. Elife 2013;2:e00792.

799 [98] Schott S, Scheuer R, Ermoli F, Glatter T, Evguenieva-Hackenberg E, Diepold A, et al. A ParDE toxin-
800 antitoxin system is responsible for the maintenance of the Yersinia virulence plasmid but not for
801 type III secretion-associated growth inhibition OPEN ACCESS EDITED BY. Front Cell Infect
802 Microbiol 2023;13:1166077.

803 [99] Schindelin J, Arganda-Carreras I, Frise E, Kaynig V, Longair M, Pietzsch T, et al. Fiji: an open-source
804 platform for biological-image analysis. Nat Methods 2012;9:676–82.

805 [100] Schmidt U, Weigert M, Broaddus C, Myers G. Cell detection with star-convex polygons. Lecture
806 Notes in Computer Science (Including Subseries Lecture Notes in Artificial Intelligence and Lecture
807 Notes in Bioinformatics) 2018;11071 LNCS:265–73.

808 [101] von Chamier L, Laine RF, Jukkala J, Spahn C, Krentzel D, Nehme E, et al. Democratising deep
809 learning for microscopy with ZeroCostDL4Mic. Nat Commun 2021.

810 [102] Spahn C, Gómez-de-Mariscal E, Laine RF, Pereira PM, von Chamier L, Conduit M, et al. DeepBacs
811 for multi-task bacterial image analysis using open-source deep learning approaches.
812 Communications Biology 2022 5:1 2022;5:1–18.

813 [103] Ovesny M, Kříž ek P, Borkovec J, ˇ vindrych ZS, Hagen GM. Bioimage informatics ThunderSTORM:
814 a comprehensive ImageJ plug-in for PALM and STORM data analysis and super-resolution imaging.
815 Bioinformatics 2014;30:2389–90.

816 [104] Bekker-Jensen DB, Martínez-Val A, Steigerwald S, Rü P, Fort KL, Arrey TN, et al. A Compact
817 Quadrupole-Orbitrap Mass Spectrometer with FAIMS Interface Improves Proteome Coverage in
818 Short LC Gradients Correspondence. Mol Cell Proteomics 2020;4:716–29.

819 [105] Demichev V, Messner CB, Vernardis SI, Lilley KS, Ralser M. Brief CommuniCation DIA-NN: neural
820 networks and interference correction enable deep proteome coverage in high throughput. Nat
821 Methods 2020.

822 [106] Glatter T, Ludwig C, Ahrné E, Aebersold R, Heck AJR, Schmidt A. Large-scale quantitative
823 assessment of different in-solution protein digestion protocols reveals superior cleavage
824 efficiency of tandem Lys-C/trypsin proteolysis over trypsin digestion. J Proteome Res
825 2012;11:5145–56.

826 [107] Ahrné E, Ahrné A, Molzahn L, Glatter T, Schmidt A. Critical assessment of proteome-wide label-
827 free absolute abundance estimation strategies. Proteomics 2013;13:2567–78.

828 [108] Heroven AK, Böhme K, Rohde M, Dersch P. A Csr-type regulatory system, including small non-
829 coding RNAs, regulates the global virulence regulator RovA of Yersinia pseudotuberculosis
830 through RovM. Mol Microbiol 2008;68:1179–95.

831 [109] Avican K, Fahlgren A, Huss M, Heroven AK, Beckstette M, Dersch P, et al. Reprogramming of
832 Yersinia from Virulent to Persistent Mode Revealed by Complex In Vivo RNA-seq Analysis. PLoS
833 Pathog 2015;11:1–28.

834 [110] Schmittgen TD, Livak KJ. Analyzing real-time PCR data by the comparative CT method. Nature
835 Protocols 2008 3:6 2008;3:1101–8.

836

837